

# UC Irvine

## Faculty Publications

### Title

Where do fossil fuel carbon dioxide emissions from California go? An analysis based on radiocarbon observations and an atmospheric transport model

### Permalink

<https://escholarship.org/uc/item/3mm578xn>

### Journal

Journal of Geophysical Research, 113(G4)

### ISSN

0148-0227

### Authors

Riley, W. J.  
Hsueh, D. Y.  
Randerson, J. T.  
[et al.](#)

### Publication Date

2008-10-01

### DOI

10.1029/2007JG000625

### Supplemental Material

<https://escholarship.org/uc/item/3mm578xn#supplemental>

### Copyright Information

This work is made available under the terms of a Creative Commons Attribution License, available at <https://creativecommons.org/licenses/by/4.0/>

Peer reviewed

# Where do fossil fuel carbon dioxide emissions from California go?

## An analysis based on radiocarbon observations and an atmospheric transport model

W. J. Riley,<sup>1</sup> D. Y. Hsueh,<sup>2,3</sup> J. T. Randerson,<sup>2</sup> M. L. Fischer,<sup>4</sup> J. G. Hatch,<sup>5</sup> D. E. Pataki,<sup>2</sup> W. Wang,<sup>6</sup> and M. L. Goulden<sup>2</sup>

Received 17 October 2007; revised 22 April 2008; accepted 7 July 2008; published 7 October 2008.

[1] Characterizing flow patterns and mixing of fossil fuel-derived CO<sub>2</sub> is important for effectively using atmospheric measurements to constrain emissions inventories. Here we used measurements and a model of atmospheric radiocarbon (<sup>14</sup>C) to investigate the distribution and fluxes of atmospheric fossil fuel CO<sub>2</sub> across the state of California. We sampled <sup>14</sup>C in annual C<sub>3</sub> grasses at 128 sites and used these measurements to test a regional model that simulated anthropogenic and ecosystem CO<sub>2</sub> fluxes, transport in the atmosphere, and the resulting  $\Delta^{14}\text{C}$  of annual grasses ( $\Delta_g$ ). Average measured  $\Delta_g$  levels in Los Angeles, San Francisco, the Central Valley, and the North Coast were  $27.7 \pm 20.0$ ,  $44.0 \pm 10.9$ ,  $48.7 \pm 1.9$ , and  $59.9 \pm 2.5\%$ , respectively, during the 2004–2005 growing season. Model predictions reproduced regional patterns reasonably well, with estimates of  $27.6 \pm 2.4$ ,  $39.4 \pm 3.9$ ,  $46.8 \pm 3.0$ , and  $59.3 \pm 0.2\%$  for these same regions and corresponding to fossil fuel CO<sub>2</sub> mixing ratios ( $C_f$ ) of 13.7, 6.1, 4.8, and 0.3 ppm.  $\Delta_g$  spatial heterogeneity in Los Angeles and San Francisco was higher in the measurements than in the predictions, probably from insufficient spatial resolution in the fossil fuel inventories (e.g., freeways are not explicitly included) and transport (e.g., within valleys). We used the model to predict monthly and annual transport patterns of fossil fuel-derived CO<sub>2</sub> within and out of California. Fossil fuel CO<sub>2</sub> emitted in Los Angeles and San Francisco was predicted to move into the Central Valley, raising  $C_f$  above that expected from local emissions alone. Annually, about 21, 39, 35, and 5% of fossil fuel emissions leave the California airspace to the north, east, south, and west, respectively, with large seasonal variations in the proportions. Positive correlations between westward fluxes and Santa Ana wind conditions were observed. The southward fluxes over the Pacific Ocean were maintained in a relatively coherent flow within the marine boundary layer, while the eastward fluxes were more vertically dispersed. Our results indicate that state and continental scale atmospheric inversions need to consider areas where mixing ratio measurements are sparse (e.g., over the ocean to the south and west of California), transport within and across the marine boundary layer, and terrestrial boundary layer dynamics. Radiocarbon measurements can be very useful in constraining these estimates.

**Citation:** Riley, W. J., D. Y. Hsueh, J. T. Randerson, M. L. Fischer, J. G. Hatch, D. E. Pataki, W. Wang, and M. L. Goulden (2008), Where do fossil fuel carbon dioxide emissions from California go? An analysis based on radiocarbon observations and an atmospheric transport model, *J. Geophys. Res.*, 113, G04002, doi:10.1029/2007JG000625.

<sup>1</sup>Earth Sciences Division, E. O. Lawrence Berkeley National Laboratory, Berkeley, California, USA.

<sup>2</sup>Earth System Science Department, University of California, Irvine, California, USA.

<sup>3</sup>Now at Department of Ecology, Evolution, and Environmental Biology, Columbia University, New York, New York, USA.

<sup>4</sup>Energy and Environment Division, E. O. Lawrence Berkeley National Laboratory, Berkeley, California, USA.

<sup>5</sup>Brightworks LLC, Portland, Oregon, USA.

<sup>6</sup>Department of Ecology and Evolutionary Biology, University of California, Irvine, California, USA.

## 1. Introduction

[2] Fossil fuel combustion is the largest anthropogenic CO<sub>2</sub> source, accounting for approximately 7.0 Pg C a<sup>-1</sup> in 2000, and increasing rapidly to over 7.9 Pg C a<sup>-1</sup> in 2004 [Marland *et al.*, 2006; Raupach *et al.*, 2007]. This combustion is associated with a range of societal and economic benefits, including transportation, electricity generation, heating, air-conditioning, and others. There are, however, many costs associated with the climate consequences of this greenhouse gas that will occur across a wide range of timescales, including impacts to agricultural productivity, sea level, water resources, terrestrial and oceanic ecosystem

health, disease propagation, and fire regimes [Parry *et al.*, 2007].

[3] Accurate quantification of fossil fuel CO<sub>2</sub> emissions is needed to properly account for these costs [Stern, 2006], aid in policy development [Parry *et al.*, 2007], improve climate prediction and climate change attribution, and facilitate atmospheric inversion approaches used to quantify contemporary anthropogenic and ecosystem C fluxes [Fan *et al.*, 1998; Gurney *et al.*, 2002; Stephens *et al.*, 2007]. Further, other primary atmospheric pollutants of interest (e.g., carbon monoxide and black carbon) are often produced concurrently with CO<sub>2</sub> and surface emissions estimates for these gases and aerosols can be improved using accurate fossil fuel CO<sub>2</sub> emissions estimates [e.g., Turnbull *et al.*, 2006]. This paper describes an approach using the <sup>14</sup>C content of annual grasses and an atmospheric transport model to characterize the impacts of spatially and temporally heterogeneous surface and atmospheric processes on fossil fuel CO<sub>2</sub> transport within and out of California.

[4] The first attempts to quantify fossil fuel CO<sub>2</sub> emissions used inventories based on proxy measurements such as fuel sales and population density [Andres *et al.*, 1996; Franco, 2002; Olivier *et al.*, 1999]. The mix of fossil fuels used varies substantially around the world. In California, fossil fuel is used for transportation (~60%), electric power generation (~16%), industry (~13%), and residences (~10%) [Bemis, 2006; Franco, 2002]. Although important in characterizing regional fossil fuel CO<sub>2</sub> emissions, the accuracy of fuel use-based emissions inventories still requires improvement [Marr *et al.*, 2002], particularly at fine spatial scales. These inventories are also potentially vulnerable to political pressure, creating the need for independent verification approaches.

[5] Another approach to estimating fossil fuel CO<sub>2</sub> emissions has been to use atmospheric measurements of radiocarbon (<sup>14</sup>C) in CO<sub>2</sub>. Because <sup>14</sup>C has a relatively short half life (~5730 years) compared to the ancient plant material from which fossil fuels are derived, carbon in fossil fuels is effectively free of <sup>14</sup>C (i.e.,  $\Delta^{14}\text{C} = -1000\text{‰}$ ). With atmospheric nuclear weapon testing, the <sup>14</sup>C content of tropospheric CO<sub>2</sub> rapidly increased and by 1963 was over 900‰ in the northern hemisphere. Following the 1963 Test Ban treaty, atmospheric  $\Delta^{14}\text{C}$  levels declined, primarily as a consequence of air-sea gas exchange, uptake by land plants, dilution from fossil fuel combustion, and radioactive decay. By 2000, atmospheric levels had dropped to about 60‰, with a rate of change of about 6‰ a<sup>-1</sup> [Levin *et al.*, 2003]. While there are important latitudinal and seasonal variations in the background atmospheric (i.e., remote marine boundary layer)  $\Delta^{14}\text{C}$ , almost all of the spatial variation over North America is due to fossil fuel CO<sub>2</sub> emissions [Hsueh *et al.*, 2007; Randerson *et al.*, 2002]. For current atmospheric CO<sub>2</sub> levels, about a 2.8‰ change in <sup>14</sup>C content is equivalent to 1 ppm fossil fuel CO<sub>2</sub> ( $\frac{(60\text{‰})(380\text{ ppm}) + (-1000\text{‰})(1\text{ ppm})}{381\text{ ppm}}$ ). Since current <sup>14</sup>C accelerator mass spectrometry measurement techniques have a precision of 2.5 to 3.0‰, measurements of the  $\Delta^{14}\text{C}$  of atmospheric CO<sub>2</sub> can be used to infer fossil fuel CO<sub>2</sub> levels to a precision of about 1 ppm.

[6] Turnbull *et al.* [2006] compared <sup>14</sup>CO<sub>2</sub>, CO, and SF<sub>6</sub> as tracers of fossil fuel CO<sub>2</sub> at two sites. They concluded that CO is limited as a tracer due to uncertainty in its CO<sub>2</sub>

emission ratio, and that, as a tracer, SF<sub>6</sub> showed large biases as compared to <sup>14</sup>CO<sub>2</sub>, possibly because of differences in the spatial pattern of surface sources. Levin *et al.* [1995] studied two sites in Germany where atmospheric <sup>14</sup>CO<sub>2</sub> and radon measurements had been made. They derived fossil fuel CO<sub>2</sub> emissions and concluded that emissions estimates derived from fuel sales substantially underestimated the seasonal amplitude, likely leading to errors in the inferred seasonal cycle of terrestrial biosphere exchange. Using a longer data record, Levin *et al.* [2003] applied a similar method at two sites to estimate fossil fuel CO<sub>2</sub> emissions. They concluded that their method compared well with bottom-up statistical emissions inventories and the seasonality of fossil fuel CO<sub>2</sub> emissions was substantially larger than previously assumed. Measurements of <sup>14</sup>C in plant biomass can be used as an integrator of spatial and temporal variability in fossil fuel CO<sub>2</sub>. Hsueh *et al.* [2007], for example, mapped patterns of <sup>14</sup>C content in an annual plant (*Zea mays*) across North America. They found that relative to the intermountain West, fossil fuel CO<sub>2</sub> mixing ratios were substantially higher in California and in the Ohio Valley.

[7] In addition to constraining surface emission estimates, accurately characterizing CO<sub>2</sub> transport out of a particular region is critical for testing larger-scale atmospheric inversions [Gurney *et al.*, 2002]. Such independent measures of fossil fuel CO<sub>2</sub> production and transport will become increasingly important as society develops regulations of regional and national GHG emissions [e.g., Schwarzenegger, 2005]. Transport of CO<sub>2</sub> within and out of California is dominated by three transport mechanisms: the large-scale Pacific High, the Great Basin High (which, in combination with the Pacific High establishes wintertime offshore Santa Ana (SA) wind conditions [Conil and Hall, 2006; Raphael, 2003]), and the high elevation jet stream. The strong westerly jet streamflow has led some investigators to hypothesize that measuring CO<sub>2</sub> mixing ratios on the west and east coasts of the contiguous U.S. will facilitate continental CO<sub>2</sub> exchange estimates [Fan *et al.*, 1998]. One goal of the present work is to test this hypothesis by studying the impact of smaller scale, more variable mechanisms (e.g., Santa Ana winds) on CO<sub>2</sub> fluxes leaving the state.

[8] As a first step toward characterizing transport of fossil fuel CO<sub>2</sub> within and out of California, we used <sup>14</sup>C measurements in annual grasses to test a model that integrates fossil fuel CO<sub>2</sub> emissions, ecosystem CO<sub>2</sub> exchanges, and atmospheric transport. We then used the model over a full year to predict the pathways by which fossil fuel CO<sub>2</sub> leaves California and their relationships with atmospheric transport processes. Our results can be used to inform atmospheric inversion measurement strategies and inventory approaches to quantifying fossil fuel CO<sub>2</sub> emissions.

## 2. Methods

### 2.1. $\Delta^{14}\text{C}$ Measurements of California C<sub>3</sub> Grasses

[9] Samples of winter annual grasses were collected at 128 sites across California at the end of the 2004–2005 growing season. Packets were sent to colleagues with a letter describing our sampling protocol. To avoid point CO<sub>2</sub> sources, samples in relatively rural areas were collected more than 3.2 km away from highways, more than 45 m

from paved roads, and more than 20 m from houses or buildings. In cities, where remote sample locations were difficult or impractical to find, samples were collected in residential streets, neighborhood parks, or abandoned parking lots. We collected samples throughout California, with relatively higher collection density in the San Francisco Bay Area, Los Angeles Basin, and Central Valley Region to explore urban to rural gradients. At each site, three separate stalks of grass were collected. All of the samples consisted of annual plants that germinated in the fall of 2004 and senesced in the spring of 2005, primarily from the genera *Bromus* and *Avena*, which are highly invasive and currently widespread throughout California.

[10] Upon arrival at UCI, samples were dried at 60–70°C for at least 48 h. Plants were then ground to pass a size 40 sieve and stored in individual vials. Samples were converted to graphite and analyzed at UC Irvine's W.M. Keck Carbon Cycle Accelerator Mass Spectrometer (KCCAMS) facility [Santos *et al.*, 2004]. To ensure that we quantified the overall accuracy and to minimize differences due to running samples in different batches (or sample wheels) on the AMS, we (1) included 6–7 primary and 6–7 secondary standards with each batch of plant samples (24–27 plant samples comprised a single batch); (2) repeatedly analyzed samples collected at five sites across different batches; and (3) used three secondary standards: barley (FIRI G; SD = 2.3‰ based on 20 replicates distributed across multiple batches), oxalic acid (SD = 3.2‰ with 5 replicates), and an Australian National University standard (SD = 2.6‰ with 5 replicates).

## 2.2. Coupled MM5, LSM1, and Atmospheric Tracer Model

[11] MM5 [Grell *et al.*, 1995] is a nonhydrostatic, terrain-following sigma-coordinate mesoscale meteorological model used in weather forecasting and in studies of atmospheric dynamics, surface and atmosphere coupling, and pollutant dispersion. The model has been applied in many studies in a variety of terrains, including areas of complex topography and heterogeneous land-cover (for a partial list: <http://www.mmm.ucar.edu/mm5/Publications/mm5-papers.html>). The following physics packages were used for the simulations shown here: Grell convection scheme, simple ice microphysics, MRF planetary boundary layer (PBL) scheme, and the CCM2 radiation package. The MRF PBL scheme [Hong and Pan, 1996] is a high-resolution PBL transport model that includes both local and non-local vertical transport. The inert tracer model follows the current MM5 transport calculations for water vapor. We tested the numerical solution of the tracer transport predictions and successfully compared predicted and measured CO<sub>2</sub> mixing ratios at the Trinidad Head station (located on the northern California coast) [Riley *et al.*, 2005].

[12] LSM1 [Bonan, 1996] is a “big-leaf” [e.g., Dickinson *et al.*, 1986; Sellers *et al.*, 1996] land-surface model that simulates CO<sub>2</sub>, H<sub>2</sub>O, and energy fluxes between ecosystems and the atmosphere. Modules are included that simulate fluxes of radiation, momentum, sensible heat, and latent heat; belowground energy and water fluxes, and coupled CO<sub>2</sub> and H<sub>2</sub>O exchange between soil, plants, and the atmosphere. Twenty-eight land surface types, comprising varying fractional covers of thirteen plant types, are simu-

lated in the model. Soil hydraulic characteristics are determined from soil texture. LSM1 has been tested in a range of ecosystems at the site level [e.g., Bonan *et al.*, 1997, 1995; Riley *et al.*, 2003]. Cooley *et al.* [2005] described the integration of LSM1 with MM5 and demonstrated that the model accurately predicted surface latent, sensible, and ground heat fluxes; near-surface air temperatures; and soil moisture and temperature by comparing model simulations with data collected during the FIFE campaign [Betts and Ball, 1998].

[13] We imposed constant atmospheric CO<sub>2</sub> mixing ratio (380 ppm) and  $\Delta^{14}\text{C}$  ( $\Delta_b = 60\text{‰}$ ) boundary conditions at the edges of the domain. In reality, there are vertical, horizontal, and temporal variations in these boundary conditions. These variations should be relatively small and we did not expect them to substantially influence model estimates of  $\Delta_g$ . Our use of constant boundary conditions had no effect on our model predictions of fossil fuel CO<sub>2</sub> transport within and out of California.

## 2.3. Fossil Fuel CO<sub>2</sub> Emissions

[14] We estimated spatially and temporally resolved fossil fuel CO<sub>2</sub> emissions by scaling fossil fuel NO<sub>x</sub> emission estimates reported in the 2002 U.S. Environmental Protection Agency's National Emissions Inventory (NEI) in a manner similar to that used for CO by Gerbig *et al.* [2003]. This approach provides finer spatial and temporal resolution than is present in available inventories of fossil fuel consumption. For our work, the NEI emission estimates were distributed at 36 km resolution by the Lake Michigan Air Directors Consortium with hourly resolution on weekdays, Saturdays, and Sundays of each month in 2002 (<http://www.ladco.org/>). The overall scaling of CO<sub>2</sub> from NO<sub>x</sub> emissions was estimated using the ratio of California's annual NO<sub>x</sub> (1600 Mg NO<sub>x</sub> a<sup>-1</sup>) to CO<sub>2</sub> (370 ± 3 Tg CO<sub>2</sub> a<sup>-1</sup>) emissions [Blasing *et al.*, 2004; EIA, 2003] for 2002. Fossil CO<sub>2</sub> emissions are concentrated in the urban centers of the Los Angeles Basin and the San Francisco Bay area, with significant emissions present in the Central Valley (Figure 1).

[15] One of the largest errors in our CO<sub>2</sub> emissions estimates was likely a result of spatial variations in the CO<sub>2</sub>:NO<sub>x</sub> emission ratio. However, the model's relatively large spatial resolution (36 km) and the expected variety of sources within this resolution (particularly in urban areas where the preponderance of CO<sub>2</sub> emissions occur) will reduce uncertainty resulting from spatial variability in emission ratios associated with different point sources. Further, although seasonal cycles of the NEI emissions inventory are specific to a given state or region, the diurnal and day-to-day temporal variations in fossil CO<sub>2</sub> emissions are characterized by national averages. These small timing errors probably have a relatively small effect on our model estimates of C<sub>f</sub>.

## 2.4. Simulation Approach

[16] We used the standard initialization procedure for MM5v3.5, which applies first-guess and boundary condition fields interpolated from the NOAA National Center for Environmental Prediction (NCEP) reanalysis data [Kalnay *et al.*, 1996; Kistler *et al.*, 2001] to the outer computational grid. The model was run with a single domain with



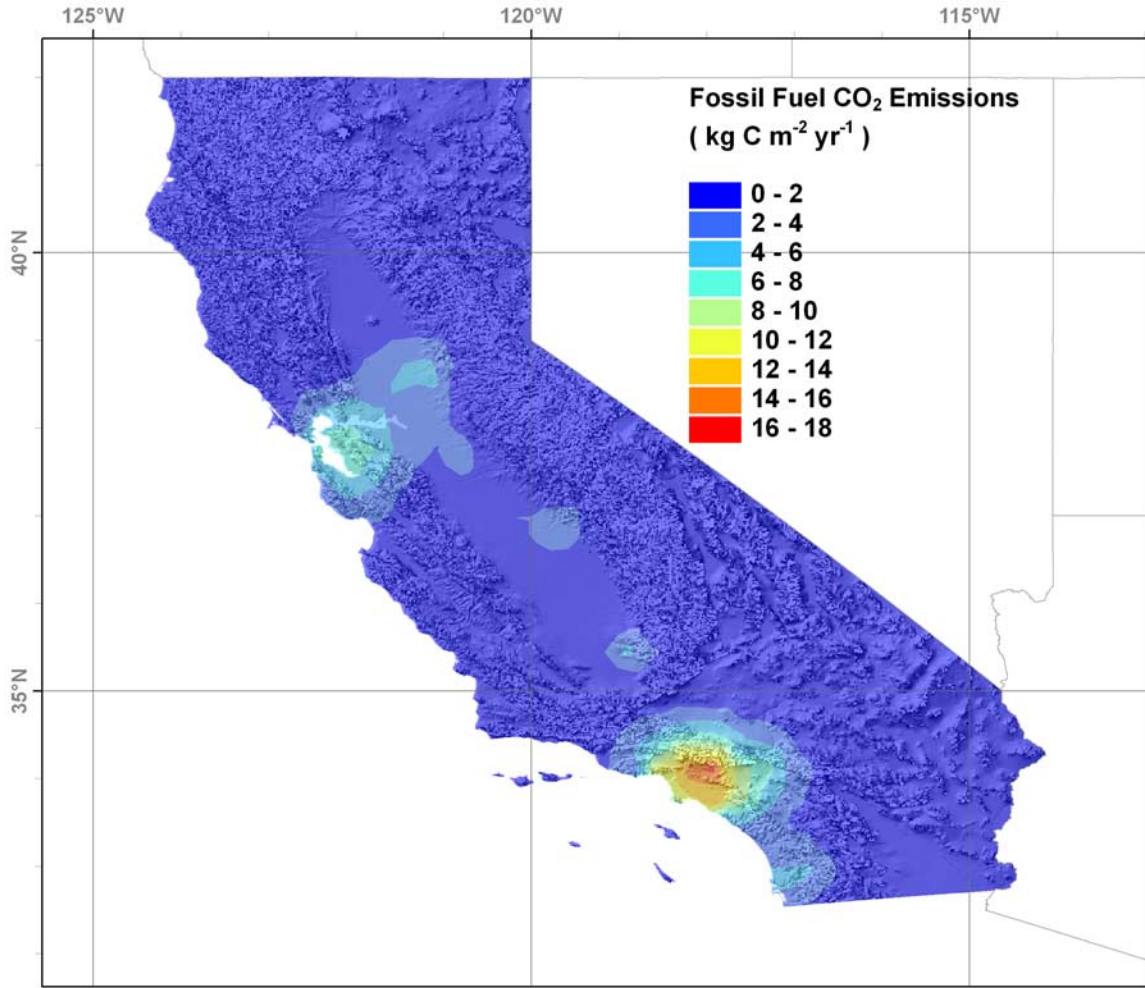


**Figure 1.** Cumulative annual fossil fuel CO<sub>2</sub> emissions (kg C m<sup>-2</sup> a<sup>-1</sup>) with the spatial pattern derived from a high resolution NO<sub>x</sub> inventory and scaled to match state-wide CO<sub>2</sub> emissions inventory. Background color interpolation was generated using the Inverse Distance Weighted (IDW) method based on 15 nearest neighbors within the Geostatistics Analyst tools in ESRI's ArcMap software.

horizontal resolution of 36 km and 18 vertical sigma layers between the surface and 5000 Pa; the time step used was 108 s, and output was generated every two hours. The two-hourly model output was used in all the analyses that follow by integrating or averaging over hourly, seasonal, or annual periods.

[17] We simulated a twelve-month period (July, 2004 through June, 2005) that encompasses the typical growing season for C<sub>3</sub> plants (November through May). The model was then run again over the same period, but with ecosystem respiration scaled by a constant factor so that the annual net CO<sub>2</sub> flux was zero at each grid cell [Denning *et al.*, 1996]. The most abundant vegetation cover type inferred from the USGS 1 km surface cover map was used to identify the dominant vegetation in each 36 × 36 km grid cell. Since many grid cells are not dominated by C<sub>3</sub> grasses, we estimated C<sub>3</sub> gross primary production (GPP,  $G_p$ ,  $\mu\text{mol m}^{-2} \text{s}^{-1}$ ) at each grid cell over the simulation period to ensure that the life history, and therefore the time history of CO<sub>2</sub> assimilation, was properly accounted for. C<sub>3</sub> grass GPP was estimated using the MM5 meteorological forcing,

the offline version of LSM1.0, and MODIS LAI profiles (<http://LPDAAC.usgs.gov>) for this time period spatially averaged over California. To ensure that the LAI profiles were representative of C<sub>3</sub> grasses, we set LAI to zero during June through October, the typical period between plant senescence and germination. Predicted grass  $\Delta^{14}\text{C}$  ( $\Delta_g$ , ‰) changed only slightly when we used GPP calculated from the LAI time series of default vegetation in the coupled model (versus using the GPP derived from MODIS LAI time series).

## 2.5. $\Delta^{14}\text{C}$ of Near-Surface CO<sub>2</sub>

[18] The  $\Delta^{14}\text{C}$  of near-surface CO<sub>2</sub> at a particular grid cell and time depends on CO<sub>2</sub> and  $^{14}\text{CO}_2$  fluxes from advection from adjacent cells, respiration, and fossil fuel combustion. Assuming that the  $\Delta^{14}\text{C}$  of respiration does not vary, a steady state mass balance gives a relationship for the  $\Delta^{14}\text{C}$  of near-surface atmospheric CO<sub>2</sub> ( $\Delta_a$ , ‰):

$$\Delta_a = \frac{\Delta_b C_b + \Delta_r C_r + \Delta_f C_f}{C_b + C_r + C_f}. \quad (1)$$

Here, the subscripts  $b$ ,  $r$ , and  $f$  refer to background, heterotrophic respiration, and fossil fuel, respectively;  $\Delta$  refers to  $\Delta^{14}\text{C}$  (‰);  $C$  refers to the atmospheric CO<sub>2</sub> mixing ratio (ppm); and  $\Delta_f = -1000$ ‰. Note that because  $\Delta^{14}\text{C}$  notation normalizes for variations in fractionation using concurrent  $^{13}\text{C}$  observations [Stuiver and Polach, 1977], fractionation by photosynthesis does not impact  $\Delta_a$ . Temporal variations in background CO<sub>2</sub> mixing ratio ( $C_b$ ) and  $\Delta^{14}\text{C}$  ( $\Delta_b$ ) occur over the year and probably introduce some error into our estimates of  $C_f$  derived from the observations via equation (1). For the model analysis, this error source is likely to be small compared to uncertainties arising from the fossil fuel emissions inventory and biases in model transport. Further, these variations will not impact our analysis of flow patterns of fossil fuel CO<sub>2</sub> emitted within California.

[19] We estimated  $\Delta_r$  by combining heterotrophic respiration impulse functions derived from the CASA model [Thompson and Randerson, 1999] and a  $\Delta^{14}\text{C}$  record of the atmosphere since 1890 [Levin and Heshaimer, 2000; Levin and Kromer, 2004]. The impulse functions were generated for an area-weighted combination of eleven biome types present in California. The area-weighted  $\Delta^{14}\text{C}$  of heterotrophic respiration was calculated to be 112‰, with a range between 101‰ for grasslands and 118‰ for evergreen needleleaf trees. Assuming that ecosystem respiration was 50% heterotrophic and approximately 50% autotrophic [Litton et al., 2007; Waring et al., 1998], and that autotrophic respiration had a  $\Delta^{14}\text{C}$  of  $\Delta_a$ , we estimated that  $\Delta_r = (60+112)/2 = 89$ ‰.

[20] We note that Turnbull et al. [2006] (their equation (1)) and Levin et al. [2003] (their equation (3)) used different relationships than equation (1) for estimating fossil fuel CO<sub>2</sub> mixing ratios based on atmospheric  $\Delta^{14}\text{C}$  measurements. The derivation of equation (1) assumes that the  $\Delta^{14}\text{C}$  of photosynthesis and autotrophic respiration are  $\Delta_a$ , while that of Turnbull et al. [2006], for example, assumed a  $\Delta^{14}\text{C}$  of photosynthesis equivalent to background air ( $\Delta_b$ ). The impact of this difference is often small, but can be as high as 0.5 ppm in the inferred value of  $C_f$ .

## 2.6. Estimating the $\Delta^{14}\text{C}$ of C<sub>3</sub> Grasses

[21] To estimate  $\Delta^{14}\text{C}$  of C<sub>3</sub> grasses ( $\Delta_g$ ), we computed the GPP-weighted sum of  $\Delta_a$  at each grid cell:

$$\Delta_g = \frac{\int_t \Delta_a G_p dt}{\int_t G_p dt}, \quad (2)$$

where the integrals are evaluated over the entire year of the simulation. Thus, the predicted biomass  $^{14}\text{C}$  composition reflects both the atmospheric  $\Delta^{14}\text{C}$  and the temporal variation in plant C assimilation. We evaluated  $\Delta_g$  with both default (i.e., using the default vegetation type and LAI time series used in LSM1.0) and satellite-derived C<sub>3</sub> grass LAI time series.

## 2.7. Near-Surface Fossil Fuel CO<sub>2</sub> Versus Local Emissions

[22] To characterize impacts of local (i.e., from the same model grid cell) fossil fuel CO<sub>2</sub> emissions on  $\Delta_a$ , we developed a non-dimensional index ( $I$ ).  $I$  is calculated,

for each grid cell, as the ratio of local surface fossil fuel CO<sub>2</sub> mixing ratio to local fossil fuel CO<sub>2</sub> emissions ( $E_f$ , kg m<sup>-2</sup> s<sup>-1</sup>) normalized by the statewide average of these quantities:

$$I = \frac{\bar{C}_f / \int_{\text{Calif}} \bar{C}_f dA}{\bar{E}_f / \int_{\text{Calif}} \bar{E}_f dA} \quad (3)$$

where the overbars indicate time averaging over the year and  $A$  represents the area of California. While this index does not give a direct measure of the impact of local versus distant sources, it allows a relative comparison between regions within the state.

## 2.8. Santa Ana Winds

[23] Santa Ana winds are an important component of southern California meteorology, partly because they substantially increase wildfire risk [Westerling et al., 2004], but also because they cause transport that opposes the prevailing eastward flow. Santa Ana events are characterized by dry and often hot offshore winds. Raphael [2003] described a 33-year record of SA occurrences and the conditions necessary for their development: a high pressure region in the Great Basin and a surface low pressure system off the Southern California coast. SA conditions occur typically between September and April, with peak occurrences in December. Conil and Hall [2006] describe three October–March southern California wind regimes (alongshore, on-shore, and offshore Santa Ana flows). They concluded that none of the large-scale teleconnection patterns (e.g., the Pacific–North American mode) are more likely than any of the others to coincide with the three southern California wind regimes.

[24] As we discuss below, Santa Ana winds substantially impact fossil fuel CO<sub>2</sub> transport toward the south and west from September to May. Further, there is large interannual variability in the number of Santa Ana days [Raphael, 2003]. To place our results for a single year into a broader context with respect to this transport mechanism, we developed a simple method to predict the number of SA wind days ( $N_S$ ) using the six-hour NCEP surface pressure and wind direction predictions. We identified Santa Ana days as those with both (1) a 3 A.M. (Pacific Standard Time) pressure difference between grid cells over the Great Basin and Interior West (lower left corner: 118°W 36°N; upper right corner: 103°W 43°N) and over the Pacific Ocean (lower left corner: 126°W 29°N; upper right corner: 114°W 35°N) that was larger than 1400 Pa and (2) winds in Los Angeles from between northerly and easterly. The predicted  $N_S$  compared well with the monthly and interannual variability estimated by Raphael [2003] (Figure 2).

## 3. Results and Discussion

### 3.1. Measured $\Delta^{14}\text{C}$ of C<sub>3</sub> Grasses

[25] Measured  $\Delta_g$  for our sample sites across California are shown in Figure 3. Additional information on site coordinates, elevation, and species type is provided in Table 1. Annual grasses growing on the coast in the northern part of the state had the highest radiocarbon levels (and thus

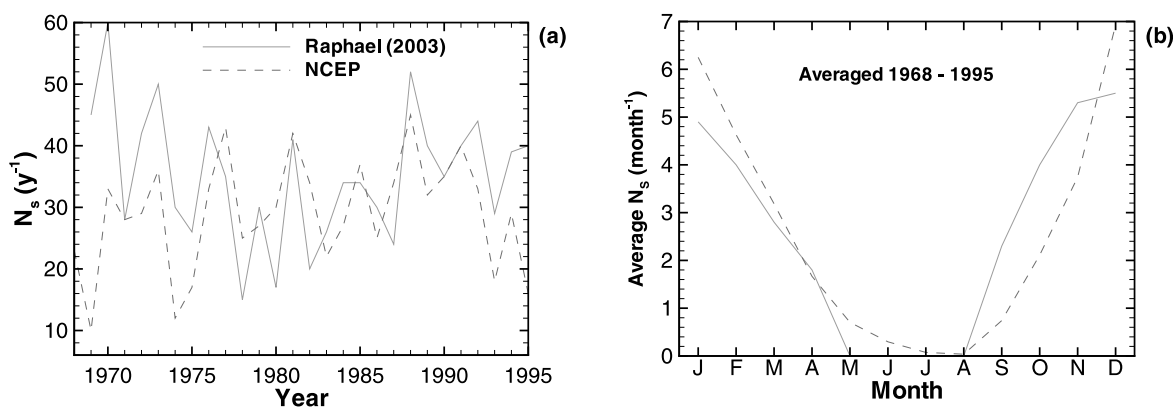


**Figure 2.** Predicted Santa Ana days per year using the NCEP reanalysis and the 28 year estimates from *Raphael* [2003]: (a) yearly total  $N_s$ ; (b) monthly average  $N_s$  between 1968 and 1995. The simple method to predict  $N_s$  using the NCEP reanalysis sea level pressure and wind direction data captures much of the monthly and interannual variability.

were exposed to the least amount of locally added fossil fuel CO<sub>2</sub>). The mean of northern coastal samples from sites near Crescent City, McKinleyville, Rohnerville, and Mendocino was  $59.5 \pm 2.1\%$ . Coastal sites in the central part of the state were also relatively clean, with a mean of  $58.2 \pm 2.7\%$  for

samples collected near Carmel, Fort Hunter-Liggett, Gorda, Los Osos, and Santa Cruz Island.

[26] Within urban areas,  $\Delta_g$  was substantially lower and more variable. For example, in the Los Angeles Basin,  $\Delta_g$  ranged from  $-14.3$  to  $60.5\%$ , with a mean of  $27.7 \pm 20.0\%$

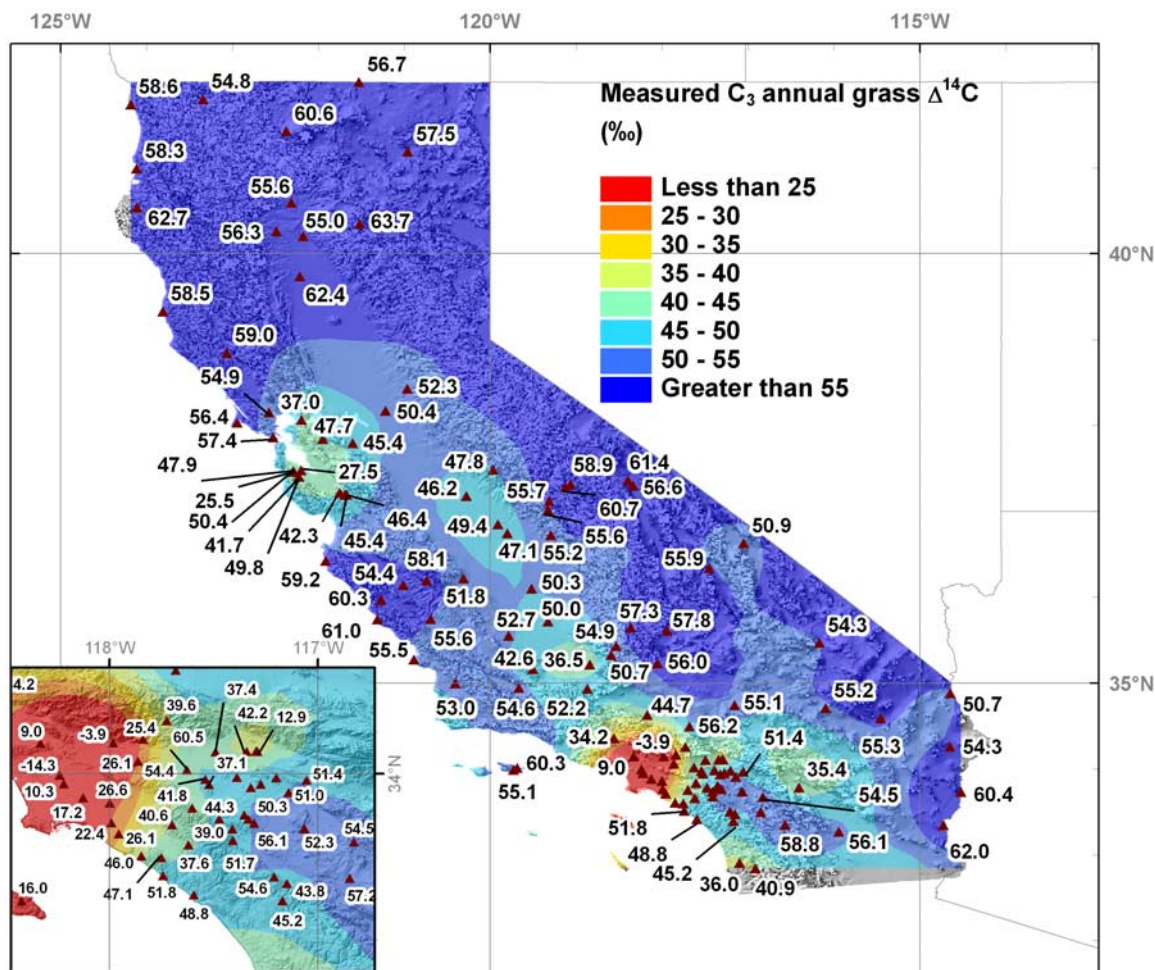


**Figure 3.** Measured  $\Delta^{14}\text{C}$  of California C<sub>3</sub> grasses ( $\Delta_g$ , ‰); (inset) expanded view of the Los Angeles Basin. Background interpolation color was built based on 13 nearest neighbors using a cokriging method (including elevation) using Geostatistics Analyst tools in ESRI's ArcMap software.



**Table 1.** Sample Locations, Measured  $\Delta^{14}\text{C}$ , and Measurement Precision (Standard Deviation) for Samples Collected in California<sup>a</sup>

Nearest City	Collection Date	Longitude	Latitude	Elevation (m)	Distance to City (km)	Species	Number of Runs	$\Delta^{14}\text{C}$ (‰)	Standard Deviation Error Estimate <sup>b</sup>
Adin	7/6/05	-120.95785	41.19023	1295	—	<i>Hordeum leporinum</i>	1	57.5	—
Ahwahnee	7/26/05	-119.32773	37.01615	710	—	<i>unk annual grass</i>	1	55.6	—
Arcadia	7/9/05	-117.98225	34.14960	177	7	<i>Bromus</i>	1	-3.9	—
Arvin	2/8/06	-118.84207	35.21518	128	1	<i>Avena</i>	3	36.5	6.6
Avalon	8/8/05	-118.42117	33.39077	19	11	<i>unk annual grass</i>	1	16.0	—
Baker	7/12/05	-116.16623	35.46982	208	25	<i>Schizmus barbatus</i>	1	54.3	—
Barstow	2/9/06	-117.15400	34.74478	902	24	<i>Bromus</i>	1	55.1	—
Bellflower	8/8/05	-118.12550	33.88620	24	0	<i>Bromus madritensis</i>	1	17.2	—
Benicia	7/5/05	-122.19520	38.06572	12	—	<i>Avena barbata</i>	1	37.0	—
Blythe	2/9/06	-114.51695	33.73420	90	19	<i>Schizmus barbatus</i>	1	60.4	—
Bodfish	2/8/06	-118.53335	35.43045	1050	23	<i>Bromus</i>	1	54.9	—
Buena Park	8/5/05	-117.99773	33.86045	30	0	<i>unk annual grass</i>	1	26.6	—
Byron	7/16/05	-121.60000	37.79500	27	7	<i>Avena</i>	1	45.4	—
Calimesa	8/7/05	-117.05319	33.97124	678	~3	<i>Bromus diandrus</i>	1	51.4	—
Calimesa	3/5/06	-117.72528	34.25628	876	<	<i>Avena</i>	1	39.6	—
Cantil	2/8/06	-118.05203	35.23307	721	11	<i>Bromus</i>	1	56.0	—
Carmel	2/18/06	-121.91424	36.42472	11	16	<i>Avena</i>	1	59.2	—
Central Weed	8/1/05	-122.37306	41.42806	1093	—	<i>Bromus</i>	1	60.6	—
Chino	8/9/05	-117.62770	34.01942	230	0	<i>Bromus madritensis</i>	1	60.5	—
Coalinga	7/10/05	-120.30927	36.21873	293	8	<i>Avena</i>	1	51.8	—
Coalinga	7/10/05	-120.73930	36.19833	708	47	<i>Avena</i>	1	58.1	—
Corcoran	2/8/06	-119.51670	36.09868	55	4	<i>Avena</i>	1	50.3	—
Corona	8/8/05	-117.60380	33.83770	406	1	<i>Bromus madritensis</i>	1	41.8	—
Corona	7/13/05	-117.47345	33.78400	317	18	<i>Bromus</i>	1	44.3	—
Covina	2/25/06	-117.86287	34.06223	309	1.6	<i>Avena</i>	1	26.1	—
Crescent City	7/72005	-124.18452	41.74062	0	1.6	<i>Avena barbata</i>	1	58.6	—
Cuyama	7/10/05	-119.66593	34.94375	675	16	<i>Avena</i>	1	54.6	—
Dana Point	8/8/05	-117.74212	33.51223	101	5	<i>Bromus madritensis</i>	1	51.8	—
Danville	7/21/05	-121.94862	37.84420	254	8	<i>Avena</i>	1	47.7	—
~ Essex	2/9/06	-115.45295	34.59003	378	25	<i>Schizmus barbatus</i>	1	55.3	—
Fallbrook	7/26/05	-119.29540	36.72597	471	—	<i>Avena</i>	1	55.2	—
Fontana	8/9/05	-117.49133	34.10668	372	0	<i>Avena fatua</i>	1	37.4	—
Fort Hunter-Liggett	2/18/06	-121.26952	35.96987	440	8	<i>unknown annual</i>	1	60.3	—
Fountain Valley	7/9/05	-117.95505	33.71373	9	0	<i>Bromus madritensis</i>	1	26.1	—
Freeman Jct.	2/8/06	-117.94177	35.61390	1144	5	<i>Schizmus barbatus</i>	1	57.8	—
in Fresno	7/10/05	-119.79985	36.74405	87	0	<i>Bromus</i>	1	47.1	—
Glendale	7/9/05	-118.33140	34.14723	154	0	<i>Lolium multiflorum</i>	5	9.0	3.0
Glendora	2/25/06	-117.83827	34.16668	414	8	<i>bromus</i>	1	25.4	—
Gorda	2/18/06	-121.31502	35.74208	21	24	<i>Briza maxima</i>	1	61.0	—
Grapevine	2/8/06	-118.87090	34.93673	397	5	<i>Avena</i>	1	52.2	—
Happy Camp	7/6/05	-123.33998	41.80170	506	8	<i>Avena sativa</i>	1	54.8	—
Hatfield	7/6/05	-121.52692	42.00005	1231	8	<i>Bromus</i>	1	56.7	—
Havilah	2/8/06	-118.59082	35.32653	662	28	<i>Avena</i>	1	50.7	—
Hemet	4/22/05	-117.06639	33.73925	494	9.6	<i>Bromus madritensis</i>	1	45.8	—
Hemet	8/7/05	-116.82757	33.67310	943	12	<i>Bromus madritensis</i>	1	54.5	—
Hemet	8/7/05	-117.06368	33.73693	561	3	<i>Bromus diandrus</i>	1	52.3	—
Herndon	7/10/05	-119.90795	36.85158	83	3	<i>Bromus</i>	1	49.4	—
Ione	7/13/05	-120.96600	38.43110	171	16	<i>Avena</i>	2	52.3	4.2
West side of Kaiser Pass	7/26/05	-119.12500	37.28333	2136	—	<i>Taeniatherum caput</i>	1	60.7	—
East side of Kaiser Pass	7/26/05	-119.06667	37.31667	2427	—	<i>Taeniatherum caput</i>	1	58.9	—
Laguna Woods	8/9/05	-117.75008	33.59867	146	1	<i>Bromus madritensis</i>	1	47.1	—
Lake Elsinore	8/7/05	-117.40906	33.68130	553	1	<i>Bromus madritensis</i>	1	51.7	—
Lake Elsinore	8/8/05	-117.41055	33.73694	388	6	<i>Bromus madritensis</i>	1	39.0	—
Littlerock	2/9/06	-117.68177	34.49850	1042	29	<i>Bromus</i>	1	56.2	—
Lodi	7/5/05	-121.21592	38.17407	16	—	<i>Avena barbata</i>	1	50.4	—
Los Osos	7/10/05	-120.88797	35.27457	4	8	<i>Bromus</i>	5	55.5	2.6
Ludlow	2/9/06	-116.09282	34.71117	571	4	<i>Schizmus barbatus</i>	1	55.2	—
Marin	9/17/05	-122.57284	38.15231	41	—	<i>Avena</i>	1	54.9	—
Mariposa	7/11/05	-119.96542	37.48633	626	12	<i>Avena</i>	1	47.8	—
McKinleyville	7/72005	-124.11443	40.99408	0	—	<i>Lolium temulentum</i>	1	58.3	—
McKittrick	2/8/06	-119.78767	35.55163	182	33	<i>Avena</i>	1	52.7	—
Mendocino	9/17/05	-123.81073	39.32847	13	—	<i>unknown annual grass</i>	1	58.5	—
Merced	7/10/05	-120.27475	37.17860	65	26	<i>Hordeum vulgare</i>	1	46.2	—
Mill Creek	8/12/05	-121.51890	40.34940	1484	5	<i>Bromus japonicus</i>	1	63.7	—
Miramar	7/13/05	-117.09843	32.90470	194	0	<i>Avena</i>	1	36.0	—
Moreno Valley	5/25/05	-117.20012	33.98249	819	6.4	<i>Bromus diandrus</i>	1	62.3	—
Moreno Valley	3/15/05	-117.27346	33.95076	593	1	<i>Bromus madritensis</i>	1	45.7	—
Moreno Valley	8/7/05	-117.13974	33.91177	503	1	<i>Bromus diandrus</i>	1	51.0	—
Morgan Hill	8/31/05	-121.68799	37.19179	132	6.4	<i>Lolium multiflorum</i>	1	45.4	—
Morgan Hill	8/31/05	-121.67296	37.19321	328	6.4	<i>Lolium multiflorum</i>	1	46.4	—



Table 1. (continued)

Nearest City	Collection Date	Longitude	Latitude	Elevation (m)	Distance to City (km)	Species	Number of Runs	$\Delta^{14}\text{C}$ (‰)	Standard Deviation Error Estimate <sup>b</sup>
Murrieta	8/7/05	-116.84678	33.50103	805	25	<i>Bromus madritensis</i>	1	57.2	–
Needles	2/9/06	-114.64537	34.88278	158	6	<i>Schizmus barbatus</i>	2	50.7	2.5
Newport Beach	8/8/05	-117.84613	33.60758	173	1	<i>Bromus madritensis</i>	1	46.0	–
Norco	8/9/05	-117.54058	33.97418	216	9.6	<i>Bromus madritensis</i>	1	54.4	–
Norco	8/7/05	-117.52191	33.94940	260	0	<i>Bromus madritensis</i>	1	37.1	–
Orland	7/7/05	-122.21670	39.74043	73	–	<i>Digitaria sanguinalis</i>	1	62.4	–
Owens Valley	6/5/05	-118.33158	37.30057	1223	–	<i>unk annual grass</i>	1	56.6	–
in Owens Valley	8/1/05	-118.39500	37.36333	1263	–	<i>Bromus</i>	1	61.4	–
Palmdale	2/9/06	-118.16923	34.63108	785	9	<i>Bromus</i>	1	44.7	–
Palo Verde	2/9/06	-114.72390	33.34572	79	10	<i>Schizmus barbatus</i>	1	62.0	–
Paramint Springs	7/12/05	-117.45012	36.33752	526	3	<i>Schizmus barbatus</i>	1	55.9	–
Perris	3/17/05	-117.35351	33.80392	605	–	<i>Amsinckia menziesii</i>	1	54.1	–
Perris	8/7/05	-117.33371	33.78429	678	8	<i>Bromus madritensis</i>	1	50.3	–
Perris	8/7/05	-117.30533	33.76430	664	6	<i>Bromus diandrus</i>	1	56.1	–
Pond	2/8/06	-119.32518	35.71778	83	16	<i>Avena</i>	1	50.0	–
Portola Valley	9/15/05	-122.22440	37.40468	182	–	<i>Lolium multiflorum</i>	1	49.8	–
Pt. Reyes Station	8/15/05	-122.94817	38.03357	36	32	<i>unk annual grass</i>	1	56.4	–
Rancho Mirage	7/13/05	-116.40618	33.78547	97	1	<i>Schizmus barbatus</i>	1	35.4	–
Racho Santa Margarita	8/8/05	-117.61981	33.65973	343	1	<i>Bromus diandrus</i>	1	37.6	–
Red Bluff	7/6/05	-122.17752	40.20748	92	–	<i>Avena barbata</i>	1	55.0	–
Redding	7/6/05	-122.31335	40.59692	180	8	<i>Avena barbata</i>	1	55.6	–
Redwood City	9/18/05	-122.20008	37.48194	3	–	<i>Lolium multiflorum</i>	1	27.5	–
Rialto	8/9/05	-117.34072	34.10775	361	0	<i>unk annual grass</i>	1	42.2	–
Riverside	3/17/05	-117.32154	33.93628	436	–	<i>Bromus madritensis</i>	1	42.9	–
Rohnerville	7/7/05	-124.11168	40.53955	15	–	<i>Avena barbata</i>	1	62.7	–
Rosewood	7/72005	-122.48723	40.26228	244	27	<i>Avena barbata</i>	1	56.3	–
Rubidoux	3/17/05	-117.38766	33.98448	279	–	<i>Avena fatua</i>	1	57.6	–
Salton City	2/9/06	-115.94055	33.27105	–60	1	<i>Schizmus barbatus</i>	1	56.1	–
San Bernardino	8/9/05	-117.29637	34.11058	322	0	<i>unk annual grass</i>	1	31.0	–
San Bernardino	7/13/05	-117.28990	34.10863	312	0	<i>Avena</i>	5	12.9	2.4
San Clemente	8/8/05	-117.59559	33.41920	112	0	<i>Bromus hordeaceus</i>	1	48.8	–
San Jose	8/31/05	-121.75235	37.22027	161	–	<i>Lolium multiflorum</i>	1	42.3	–
San Lucas	7/10/05	-121.01132	36.14435	144	3	<i>Avena</i>	1	54.4	–
San Miguel	7/10/05	-120.69423	35.74785	181	1	<i>Avena</i>	1	55.6	–
Santa Barbara	10/14/05	-119.72917	33.99111	214	48	<i>Avena</i>	1	55.1	–
Santa Barbara	10/14/05	-119.68333	34.01667	5	45	<i>Avena</i>	1	60.3	–
Santa Clarita	7/9/05	-118.55902	34.35702	419	4	<i>Avena</i>	1	34.2	–
Santa Maria	7/10/05	-120.40663	34.99782	126	7	<i>Avena</i>	1	53.0	–
Santee	7/13/05	-116.91053	32.84298	174	9	<i>Avena</i>	1	40.9	–
Sausalito	7/15/05	-122.52396	37.86028	219	8	<i>Avena fatua</i>	1	57.4	–
Shaver Lake	7/27/05	-119.31436	37.12405	1242	–	<i>unk annual grass</i>	1	55.7	–
Sonoma	9/17/05	-123.06633	38.84715	326	–	<i>Avena</i>	1	59.0	–
South Gate	8/8/05	-118.21920	33.95273	3	0	<i>Bromus madritensis</i>	1	10.3	–
Stovepipe Wells	7/12/05	-117.04902	36.63032	–29	5	<i>Schizmus barbatus</i>	1	50.9	–
Taft	2/8/06	-119.50445	35.16392	335	6	<i>Avena</i>	1	42.6	–
Temecula	7/13/05	-117.16952	33.39142	250	14	<i>Avena</i>	1	45.2	–
Temecula	8/7/05	-117.20937	33.50553	465	4	<i>Bromus diandrus</i>	1	54.6	–
Temecula	8/7/05	-117.14887	33.47469	409	2	<i>Bromus madritensis</i>	1	43.8	–
Tustin	8/8/05	-117.69870	33.75607	270	7	<i>Bromus diandrus</i>	1	40.6	–
Vernon	8/8/05	-118.23850	33.99487	55	0	<i>Avena fatua</i>	1	–14.3	–
Vidal Junction	2/9/06	-114.64760	34.26485	374	10	<i>Schizmus barbatus</i>	1	54.3	–
Warner Springs	7/2/05	-116.56667	33.35000	1484	3.2	<i>Avena</i>	1	58.8	–
Weldon	2/8/06	-118.36115	35.64758	804	9	<i>Bromus</i>	1	57.3	–
Westminister	8/5/05	-117.99008	33.76538	17	0	<i>Bromus hordeaceus</i>	1	22.4	–
Woodside	9/12/05	-122.29592	37.46197	135	–	<i>Lolium multiflorum</i>	1	50.4	–
Woodside	9/12/05	-122.29138	37.46422	168	3.2	<i>Lolium multiflorum</i>	1	41.7	–
Woodside	9/12/05	-122.29029	37.46467	172	3.2	<i>Lolium multiflorum</i>	1	25.5	–
Woodside	9/12/05	-122.28527	37.46197	203	–	<i>Lolium multiflorum</i>	1	47.9	–

<sup>a</sup>The pooled mean standard deviation across sites for which we made multiple measurements was 3.5‰.

<sup>b</sup>We used barley (FIRI G) as a secondary standard, and its standard deviation was 2.3‰ based on 20 replicates scattered across multiple batches. The two other secondary standards we used were an oxalic acid (OX-II) and an Australian National University (ANU) standard. These had standard deviations of 3.2‰ (with 5 replicates) and 2.6‰ (with 5 replicates), respectively. Based on the accuracy of these three standards (FIRI G, OX-II, and ANU), we assumed that the accuracy of an individual measured was  $\pm 2.7$ ‰.

(Table 2). Samples collected near the center of the Los Angeles metropolis, including those near the cities of Vernon, South Gate, Bellflower, Buena Park, and Westminster, had a mean of  $19.1 \pm 2.1$ ‰. Relative to the mean  $\Delta_g$

from the north coast (and assuming  $C_a$  equal to 380 ppm), these cities near the center of the Los Angeles metropolis had  $15.1 \pm 5.5$  ppm of locally added CO<sub>2</sub> (weighted by diurnally and seasonally varying photosynthetic C uptake).

**Table 2.** Predicted and Measured Mean (SD)  $\Delta_g$  and GPP-Weighted  $C_f$ -Inferred From Measured  $\Delta_g$  for Four Regions: North Coast, San Francisco Bay Area, Los Angeles Basin, and Central Valley<sup>a</sup>

	North Coast	San Francisco	Central Valley	Los Angeles
Measured mean (SD) $\Delta^{14}\text{C}$ (‰)	59.9 (2.5)	44.0 (10.9)	48.7 (1.9)	27.7 (20.0)
Predicted mean (SD) $\Delta^{14}\text{C}$ (‰)	59.3 (0.2)	39.4 (3.9)	46.8 (3.0)	27.6 (2.4)
Predicted mean (SD) GPP-weighted $C_f$ (ppm)	0.3 (0.08)	6.1 (1.1)	4.8 (0.9)	13.7 (0.4)

<sup>a</sup>Measured means in Los Angeles do not include February samples measured near freeways, as described in text.

In contrast, urban and suburban samples collected near the coast to the west and south of Los Angeles had markedly less exposure to fossil fuel CO<sub>2</sub>. The mean  $\Delta_g$  of samples from Newport Beach, Dana Point, and Laguna Woods was  $48.3 \pm 3.1\text{‰}$ . The relative depletion of  $\Delta_g$  for these coastal samples as compared with those from Central and Northern California may reflect (1) local fossil fuel sources that offset the cleansing impact of onshore winds and (2) entrainment of fossil fuel CO<sub>2</sub> from Los Angeles into the land-sea circulation and subsequent along-shore transport and on-shore flow [e.g., Riley *et al.*, 2005].

[27] In the San Francisco Bay region, measured  $\Delta_g$  ranged from 25.5 to 57.4‰, with a mean of  $44.0 \pm 10.1\text{‰}$ . Two samples collected along the peninsula (Redwood City and Woodside) had values below 28‰ and one sample collected along the transportation corridor near the Sacramento Delta had a  $\Delta^{14}\text{C}$  of 37.0‰. Samples from grassland parks south of San Jose were also relatively depleted with a mean of  $44.7 \pm 2.1\text{‰}$ , probably as a result of the trapping of fossil fuel CO<sub>2</sub> from San Jose between the two roughly parallel southwest to northeast coastal mountain ranges.

[28] Within the Central Valley, measured  $\Delta_g$  was lowest directly to the east of the San Francisco Bay area and increased both to the north and south. These gradients are consistent with transport and mixing of San Francisco Bay area and Sacramento fossil fuel CO<sub>2</sub> sources within the valley. The mean of samples collected to the east of the Bay Area (and including those collected near Lodi, Byron, Mariposa, Merced, and Fresno) was  $47.7 \pm 1.9\text{‰}$ . Samples collected from the northern part of the Central Valley (including samples near Redding, Rosewood, Mendocino, Orland, Red Bluff, and Mill Creek) were considerably more enriched in  $^{14}\text{C}$ , with a mean of  $58.6 \pm 3.7\text{‰}$ .

[29] There were strong gradients in  $\Delta_g$  for transects starting in the Central Valley and terminating in the Sierra. The first such transect started near Corcoran (elev. 55 m) in the middle of the Central Valley and ended near Kaiser Pass (elev. 2136 m).  $\Delta_g$  increased monotonically from 50.3 to 60.7‰ for 6 samples collected across this elevation gradient. A second transect further south ran from Arvin to Welden, and spanned about a 20‰ gradient. The increase in  $\Delta_g$  with elevation along the western slope of the Sierra was likely caused by dilution of Central Valley air (with high fossil fuel CO<sub>2</sub> mixing ratios) with air from the free troposphere. Diurnal upslope and downslope flows along the western slope of the Sierra also probably influenced  $\Delta_g$  [Dillon *et al.*, 2002]. Several studies have reported analogous elevation patterns for air pollutants transported from the Los Angeles Basin, including large nitrogen deposition [Fenn and Bytnerowicz, 1997; Fenn *et al.*, 2000] and ozone concentration [Lee *et al.*, 2003; Miller *et al.*, 1986] gradients across the San Bernardino Mountains. This pollution gra-

dient has caused significant and well-documented changes in the physiology and ecology of montane forests in this region [Arbaugh *et al.*, 1998; Fenn *et al.*, 1996; Grulke *et al.*, 1998; Grulke and Balduman, 1999; Grulke *et al.*, 2001; Miller *et al.*, 1998].

### 3.2. Predicted $\Delta^{14}\text{C}$ of C<sub>3</sub> Grasses

[30] Model estimates of  $\Delta_g$  (Figure 4) captured much of the observed spatial variability (Figure 3). Care should be taken in comparing these two contour plots because of difficult-to-quantify uncertainties introduced from our interpolation approach. Predicted mean values of  $\Delta_g$  for Los Angeles, San Francisco, the Central Valley, and the North Coast were similar to observed values (Table 2).

[31] Within the Los Angeles basin, the eastward propagation of the fossil fuel CO<sub>2</sub> plume from Los Angeles was relatively well represented. Within the San Francisco Bay region, mean predicted and measured  $\Delta_g$  differed by 5‰. The model over predicted the fossil fuel CO<sub>2</sub> mixing ratios (and depletion of  $\Delta_g$ ) to the east and north of the San Francisco Bay region within the Central Valley. It was not possible from our simulations to determine if the over prediction occurred because of errors associated with transport processes or CO<sub>2</sub> emissions estimates.

[32] Model estimates of annual mean  $\Delta^{14}\text{C}$  of near-surface atmospheric CO<sub>2</sub> ( $\Delta_a$ ; not shown) were almost the same as those of predicted  $\Delta_g$ . In Los Angeles, where  $\Delta_a$  and  $\Delta_g$  were largely impacted by local emissions, the covariance of nighttime fossil fuel CO<sub>2</sub> emissions and small PBL depths led to lower annual mean  $\Delta_a$  than  $\Delta_g$ . Similar mechanisms impacted Central Valley  $\Delta_a$  and  $\Delta_g$ . Also, some of the fossil fuel CO<sub>2</sub> emitted during the daytime in Central Valley urban areas moves laterally into rural parts of the Central Valley during the evening and night, further enhancing the differences between  $\Delta_a$  and  $\Delta_g$  in this region. To illustrate these interactions, the annual average difference between midnight and noon surface fossil fuel CO<sub>2</sub> mixing ratios were 0.02, 0.1, 2.8, and 1.4 ppm in the Coastal North, San Francisco Bay, Los Angeles, and Central Valley regions, respectively. The relatively higher nighttime fossil fuel CO<sub>2</sub> mixing ratios in Los Angeles and the Central Valley are consistent with the lower predicted value for annual mean  $\Delta_a$  as compared with  $\Delta_g$  in these regions.

[33] The impacts of boundary layer dynamics on the relationship between fossil fuel CO<sub>2</sub> emissions,  $\Delta_a$ , and  $\Delta_g$  are substantial. For example, during the summer in Los Angeles, when fossil fuel CO<sub>2</sub> emissions are relatively high, the Pacific High often causes low daytime boundary layer depths. This lowering of the effective atmospheric mixing volume enhances the impact of fossil fuel emissions on  $\Delta_a$  and  $\Delta_g$ . Concurrent changes in mixing rates between the PBL and overlying free troposphere may also be important. Figure 5 illustrates the relationship between monthly mean

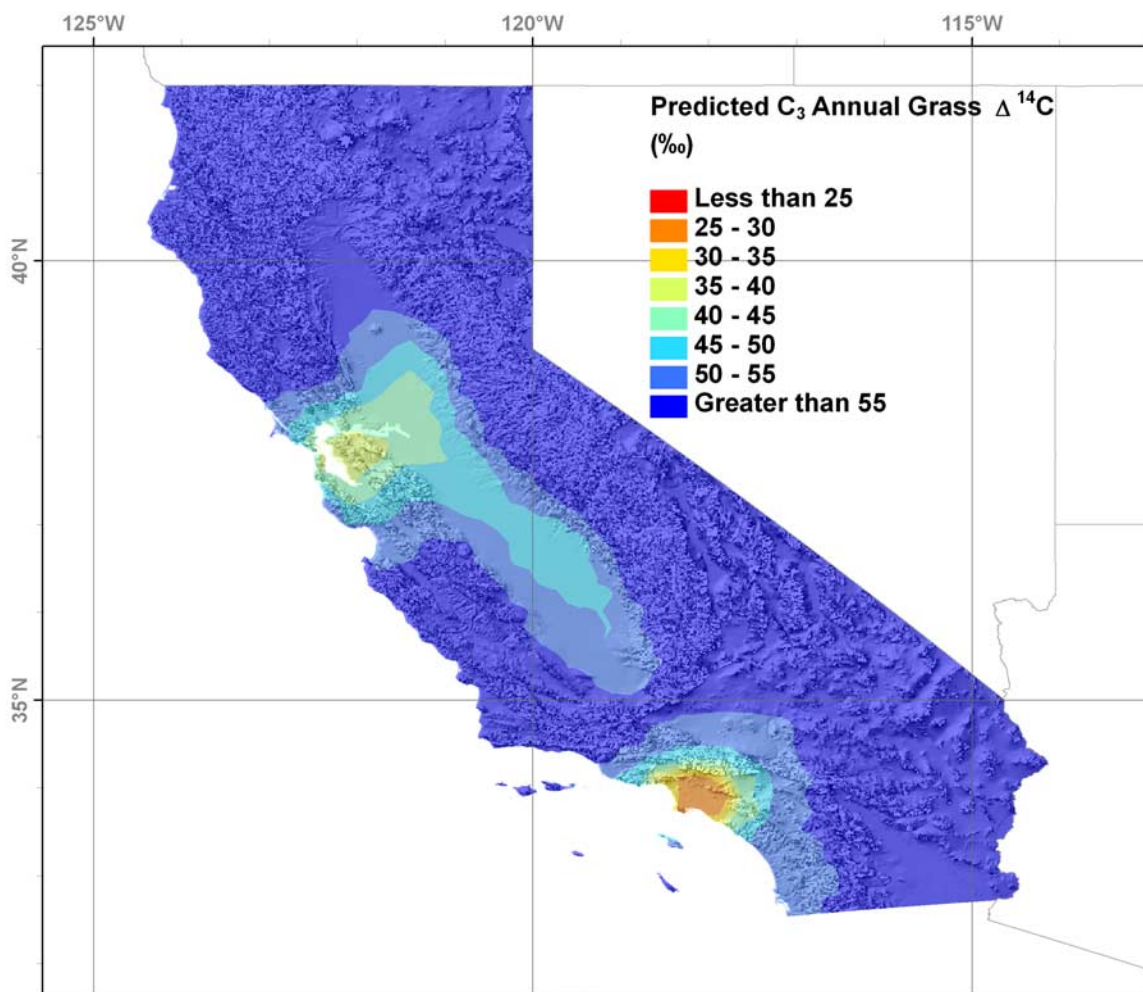


**Figure 4.** Predicted  $\text{C}_3$   $\Delta^{14}\text{C}$  ( $\Delta_g$ , ‰) averaged over the growing season, calculated as the gross primary production-weighted  $\Delta^{14}\text{C}$  of surface-layer atmospheric  $\text{CO}_2$ . Background color interpolation was generated using the same method as Figure 3.

noon fossil fuel  $\text{CO}_2$  emissions, PBL depth,  $C_f$  and  $\Delta_a$  for a single point (34 °N, 118 °W) in the Los Angeles Basin. For this point, there is a strong correlation between  $C_f$ , PBL depth, and  $\Delta_a$ . To illustrate the impact of PBL depth, we compared April and August conditions using monthly means. Between these months, fossil fuel  $\text{CO}_2$  emissions increased about 0.8%, midday PBL depth decreased about 60%,  $C_f$  increased by  $\sim 8$  ppm (170%), and  $\Delta_a$  decreased by 19‰ (from 47‰ to 28‰). This simple comparison indicates that, in Los Angeles, a substantial portion of the changes in  $C_f$  and  $\Delta_a$  between these months resulted from changes in PBL properties. Therefore, the impact of intra-annual variations in PBL dynamics must be accounted for when using  $\Delta_g$  to infer fossil fuel  $\text{CO}_2$  emissions.

[34] Measured  $\Delta_g$  were more spatially heterogeneous than predicted  $\Delta_g$  in urban areas (Table 2), likely because of spatial resolution limits associated with the meteorological model and the fossil fuel emissions inventory, both of which had a 36 km horizontal resolution. This relatively coarse spatial resolution would not resolve many topographical features, such as small valleys, which might trap fossil fuel  $\text{CO}_2$ . Also, fine scale  $\text{CO}_2$  emissions (e.g., associated with freeways and industrial point sources) were not re-

solved in our emissions estimates. However, the mean predictions accurately reproduced the patterns in measured  $\Delta_g$ , with the means differing by 0.6, 4.6, 0.1, and 1.9‰ in the North Coast, San Francisco Bay, Los Angeles, and Central Valley regions, respectively (Table 2). The mean predicted GPP-weighted fossil fuel  $\text{CO}_2$  mixing ratios are 0.3 (0.08), 6.1 (1.1), 13.7 (0.4), and 4.8 (0.9) ppm for the same regions.

### 3.3. Near-Surface Fossil-Fuel $\text{CO}_2$ Mixing Ratios Versus Local Emissions

[35] The index  $I$  (equation (3)) qualitatively describes the extent to which factors (e.g., transport, local mixing conditions) other than local emissions effect local near-surface fossil fuel  $\text{CO}_2$  mixing ratios. Since fossil fuel  $\text{CO}_2$  is a good tracer (on moderate spatial and temporal scales) of primary combustion-generated pollutants, this index may also be helpful in attributing other air pollution issues (e.g., particulate matter, tropospheric  $\text{O}_3$ ) to local versus distant sources.

[36] Predicted values of  $I$  were relatively larger in portions of the western Central Valley, Sierra Mountains, Owens Valley, and Northern California (Figure 6). Large



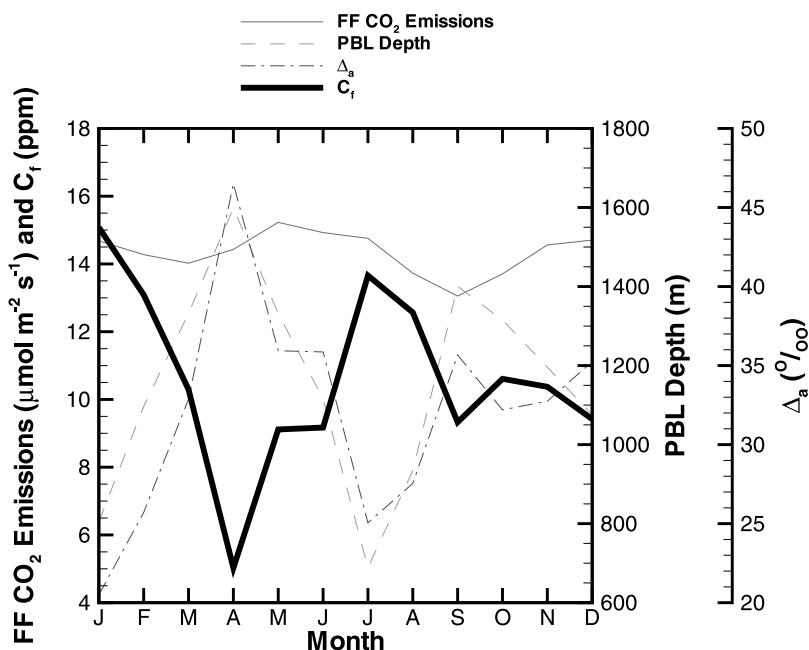


**Figure 5.** Comparison for a single model point in Los Angeles (34°N, 118°W) of midday fossil fuel CO<sub>2</sub> emissions (left axis), fossil fuel CO<sub>2</sub> mixing ratio (left axis), PBL depth (first right axis), and  $\Delta_a^{14}\text{C}$  of near-surface air (second right axis,  $\Delta_a$ ).  $\Delta_a$  is largely in phase with PBL depth and out of phase with fossil fuel CO<sub>2</sub> emissions.

values of  $I$  in the Sierra Mountains and Owens Valley occurred because very little fossil fuel CO<sub>2</sub> is emitted in these areas, yet near-surface fossil fuel CO<sub>2</sub> mixing ratios can become elevated from CO<sub>2</sub> transport from the urban air basins and the Central Valley. Fossil fuel CO<sub>2</sub> was also predicted to move from Los Angeles down the Coachella and Imperial Valleys, where fossil fuel emissions are lower. A second Southern California region just east of San Diego also had relatively larger values of  $I$ , again resulting from transport from San Diego and relatively low local emissions. These results indicate that a number of areas in California are exposed to higher primary air pollution concentrations than would result from local emissions alone.

### 3.4. Exit Pathways for California's Fossil Fuel CO<sub>2</sub>

[37] A three-dimensional representation of fossil fuel CO<sub>2</sub> leaving the California airspace is shown in Figure 7. On an annual basis, a large fraction of fossil fuel CO<sub>2</sub> exited California to the south and within the marine boundary layer (Figure 8a). A broad and more diffuse plume exited to the east, with relative maxima at latitudes corresponding approximately to Los Angeles, the middle of the Central Valley, and the San Francisco Bay area (Figure 8b). Annually, about 21, 39, 35, and 5% of fossil fuel CO<sub>2</sub> left the California airspace to the north, east, south, and west, respectively. We note that, because of the limited boundary of our simulation domain, our analysis framework is unable to characterize whether CO<sub>2</sub> exiting in any particular direction could be recirculated back into the California airspace. Given the large-scale atmospheric circulation associated with the Pacific High that results in transport of CO<sub>2</sub> from North America to Hawaii [Lintner *et al.*,

2006], we believe this recirculation to be small for air exiting to the west and south.

[38] The predicted large fraction of fossil fuel CO<sub>2</sub> leaving California to the south has important implications for continental scale inversions used to infer fossil fuel and ecosystem CO<sub>2</sub> fluxes. Future measurements of CO<sub>2</sub> and its isotopes on the islands offshore from southern California could help better characterize this transport pathway. East-west aircraft transects in the marine boundary layer near the U.S. - Mexico border (and extending several hundred kilometers offshore) would also be helpful in this regard. A second, and smaller, predicted southward flux of fossil fuel CO<sub>2</sub> occurred further east (approximately between 114°W and 115°W), also primarily within the boundary layer (Figure 8a). This portion of the flux resulted from eastward transport of fossil fuel CO<sub>2</sub> out of Los Angeles and San Diego, and then southward transport down the Coachella and Imperial Valleys. Unfortunately, we lacked measurements in these valleys to corroborate model predictions.

[39] Some of the flux moving eastward out of the Los Angeles Basin escaped directly toward Arizona, resulting in coherent fossil fuel CO<sub>2</sub> plumes centered just north of the Mexican border (Figure 8b). Much of the remaining eastward flux manifested as a broad and more diffuse plume over the Sierra Nevada. Peaks in this broad plume associated with Los Angeles (between about 33° and 36° N) and the Central Valley (between about 35° and 36° N) were discernible. In contrast to the southward fossil fuel CO<sub>2</sub> plume, the eastward plume extended further upward into the atmosphere. Of the 21% of fossil fuel CO<sub>2</sub> that left the California airspace via the north, most was centered on 122°W (approximately due north of the San Francisco Bay



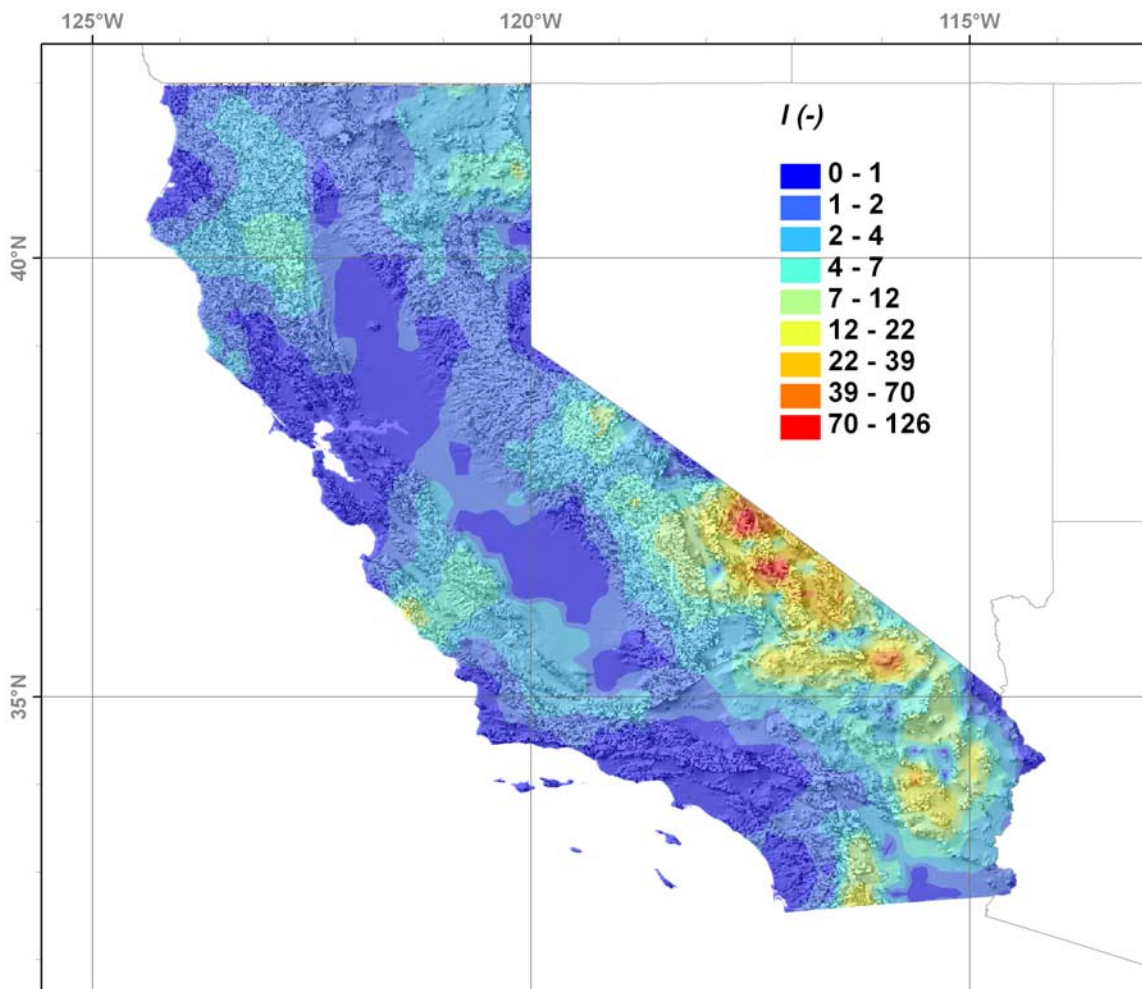


**Figure 6.** The index,  $I$ , indicating the ratio of local fossil fuel CO<sub>2</sub> (normalized by the state-wide average mixing ratio) to local fossil fuel CO<sub>2</sub> emissions (normalized by the state-wide total inventory). Areas with  $I$  larger than one have fossil fuel CO<sub>2</sub> contributions from other regions in the state (that exceed what would be expected from local emissions). Background color interpolation was generated using the same method as Figure 3.

region). Very little fossil fuel CO<sub>2</sub> (5%) exited the airspace to the west.

[40] There were distinct seasonal patterns of fossil fuel CO<sub>2</sub> fluxes in the four compass directions (Figure 9). The fraction of the monthly flux leaving toward the south had a maximum in November, with a secondary peak in March. Northward fluxes peaked in December and January while the westward flux peaked one month later in February. The eastward fluxes peaked in the summer and were relatively smaller during winter. Between November and March, the northward fluxes were roughly out of phase with the southward fluxes, implying a trade-off in transport patterns during these months.

[41] The fraction of each month's fossil fuel CO<sub>2</sub> flux leaving toward the east and west and the monthly number of Santa Ana wind days ( $N_S$ ) predicted from the NCEP reanalysis data were correlated; correlation coefficients ( $p$  value) were:  $-0.56$  ( $0.06$ ) and  $0.70$  ( $0.01$ ) for the east and west directions, respectively. Almost none of the annual cumulative flux exited toward the west outside of the Santa Ana winds season. Our one-year simulation (during 2004–

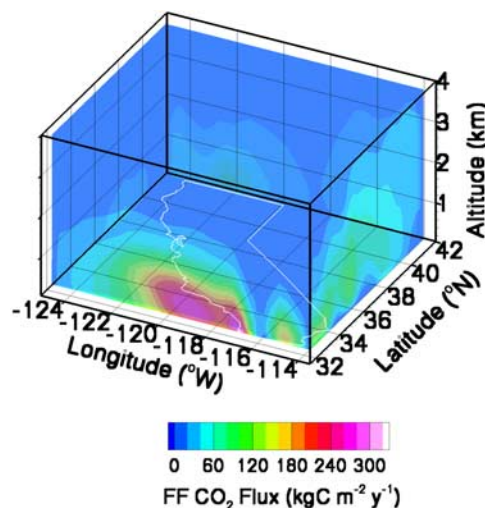


**Figure 7.** Cumulative annual fossil fuel CO<sub>2</sub> transport out of California. The figure shows contour plots on each vertical face of the cube surrounding California.

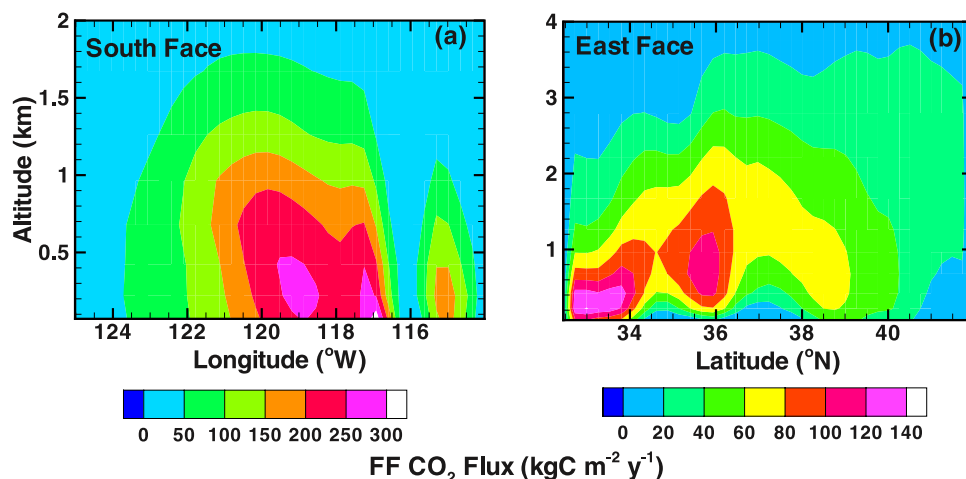


**Figure 8.** Cumulative annual fossil fuel CO<sub>2</sub> transport out of California for the (a) south and (b) east vertical faces of the cube surrounding California. Note the different altitude scales and contour intervals.

2005) does not allow us to directly infer interannual variability in the directional partitioning of fossil fuel CO<sub>2</sub> fluxes out of the state. However, since intra-annual variability in partitioning was correlated to Santa Ana wind conditions, we conclude from our simple interannual  $N_S$  estimates (Figure 2) that the relative proportion of fossil fuel CO<sub>2</sub> leaving California in each of the four directions can vary substantially between years. More work needs to be performed to characterize the impact of these short duration and intermittent events on atmospheric transport of fossil fuel derived CO<sub>2</sub>.

[42] These results are also relevant to tropospheric air quality issues and for characterizing the net climate impact of fossil fuel combustion. Tropospheric air quality can be deleteriously impacted by fossil fuel combustion, with consequent impacts to human health [Peel *et al.*, 2005; Schwartz *et al.*, 1996], vegetation [Davison and Barnes, 1998], precipitation [Rosenfeld and Givati, 2006], the Earth's radiation budget [Ramanathan *et al.*, 2001], and snow albedo and the timing of snowmelt [Flanner *et al.*, 2007]. Although atmospheric pollutant generation and transport has been the focus of many California air quality studies [e.g., Blumenthal *et al.*, 1978; Carreras-Sospedra *et*

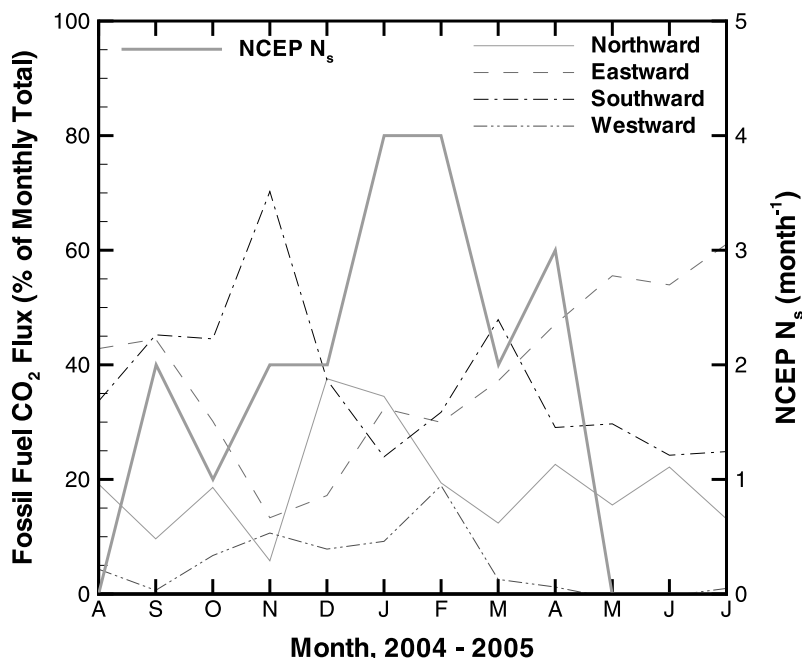


**Figure 9.** Percent of monthly fossil fuel CO<sub>2</sub> leaving the California airspace in each of the four directions (left axis) and the number of Santa Ana days each month ( $N_S$ ) predicted from the NCEP reanalysis data (right axis). Westward CO<sub>2</sub> flux and  $N_S$  were positively correlated ( $r = 0.70$ ;  $p = 0.01$ ) and eastward CO<sub>2</sub> flux and  $N_S$  were negatively correlated ( $r = -0.56$ ;  $p = 0.06$ ).

al., 2006; Croes and Fujita, 2003; Dillon et al., 2002; Edinger, 1973; Lu and Turco, 1995; McElroy and Smith, 1986; Rinehart et al., 2006], much less is known about transport of pollutants out of the state. Characterizing whether pollutants generated in California move toward Arizona, Nevada, the Pacific Ocean, or Mexico is important for characterizing the broader implications of California's fossil fuel combustion, including consequences for aerosol radiative forcing and the albedo of snow in the Sierra-Nevada and Rocky Mountain systems. For example, California emissions of black carbon aerosols, which can have a relatively short atmospheric residence time, will have a different impact on climate if they are lofted above the bright Arizona desert as compared with transport over the much darker Pacific Ocean.

#### 4. Conclusions

[43] Our prediction that 21, 39, 35, and 5% of California's fossil fuel CO<sub>2</sub> exits to the north, east, south, and west, respectively, has several important implications. Proposals have been made to use CO<sub>2</sub> measurements on the coastal boundaries of the continental U.S. to infer CO<sub>2</sub> emissions and exchanges [Wofsy and Harris, 2002]. Our estimate that a substantial portion of California's fossil fuel CO<sub>2</sub> emissions exit California toward the south implies that flask networks need to sample this plume. Since there are relatively few islands in the southward transport path, regular measurements on ships or buoys may be required. Further, many current global and regional models do not accurately simulate boundary layer development and exchanges with the free troposphere [Stephens et al., 2007], processes critical to interpreting these proposed measurements.

[44] Our results are relevant to other atmospheric components of interest. Pollutants generated concurrently with CO<sub>2</sub> or from atmospheric photochemical reactions will be impacted by the transport patterns described here. Issues relevant to tropospheric air quality include characterizing southward transport into Mexico of ozone, NO<sub>x</sub>, particulate matter, and acid compounds, and how these fluxes impact local ecosystems, visibility, and human health.

[45] Model predictions indicated that some areas within California had higher near-surface fossil fuel CO<sub>2</sub> mixing ratios than would be expected from local emissions alone. The additional fossil fuel CO<sub>2</sub> loading resulted from transport of fossil fuel CO<sub>2</sub> generated in the San Francisco Bay, Sacramento, and Los Angeles air basins. Similar behavior of other contaminants co-emitted with fossil fuel CO<sub>2</sub>, or secondary pollutants associated with combustion byproducts, would analogously be expected to contribute to air pollution in these areas.

[46] It is likely that ecosystem respiratory and photosynthetic CO<sub>2</sub> fluxes also have substantial southward flux components. Finally, given the significant correlation between southern California wildfires and Santa Ana winds, it is likely that a large fraction of wildfire CO<sub>2</sub> exits the California airspace to the south. Overall, our results indicate that the paradigm that California's air pollutants travel predominantly from west to east across the continental U.S. needs to be reexamined.

[47] **Acknowledgments.** We would like to thank the following people for collecting plant samples for us: B. Adamus, P. Adamus, D. Baldocchi, M. S. Carbone, A. M. Delaney, L. Feinstein, D. T. Fischer, M. L. Fischer, J. G. Hatch, F. M. Kai, P. G. Kennedy, L. E. Koteen, E. A. Lyons, M. and R. Lyons, R. Redmond, A. V. Rocha, D. L. Serio, J. K. Shake, M. V. Talluto, S. E. Trumbore, and S. Weiss. J. G. Hatch was supported by a Summer Undergraduate Research Education internship at LBNL through the DOE Global Change Education Program. We also wish to thank M. V. Talluto, P. A. Bowler, and M. A. Elvin for identifying grass samples; and Y. Fung for characterizing the  $\Delta^{14}\text{C}$  of respiration. NCEP Reanalysis data provided by the NOAA/OAR/ESRL PSD, Boulder, Colorado, USA, from their Web site at <http://www.cdc.noaa.gov/>. We gratefully acknowledge support from NASA (NNG05GD126), the Office of Science, U.S. Department of Energy (DE-AC02-05CH11231), and the National Science Foundation (0620176).

#### References

- Andres, R. J., G. Marland, I. Fung, and E. Matthews (1996), A  $1^\circ \times 1^\circ$  distribution of carbon dioxide emissions from fossil fuel consumption and cement manufacture, *Global Biogeochem. Cycles*, **10**, 419–430, doi:10.1029/96GB01523.
- Arbaugh, M. J., P. R. Miller, J. J. Carroll, B. Takemoto, and T. Procter (1998), Relationships of ozone exposure to pine injury in the Sierra Nevada and San Bernardino Mountains of California, USA, *Environ. Pollut.*, **101**, 291–301, doi:10.1016/S0269-7491(98)00027-X.
- Bemis, G. (2006), Inventory of California greenhouse gas emissions and sinks: 1990–2004, Calif. Energy Comm., Sacramento.
- Betts, A. K., and J. H. Ball (1998), FIFE surface climate and site-average dataset 1987–89, *J. Atmos. Sci.*, **55**, 1091–1108, doi:10.1175/1520-0469(1998)055<1091:FSCASA>2.0.CO;2.
- Blasing, T. J., C. T. Broniak, and G. Marland (Eds.) (2004), Estimates of annual fossil-fuel CO<sub>2</sub> emitted for each state in the U. S. A. and the District of Columbia for each year from 1960 through 2001, Carbon Dioxide Inf. Anal. Cent., Oak Ridge Natl. Lab., U. S. Dep. of Energy, Oak Ridge, Tenn.
- Blumenthal, D. L., W. H. White, and T. B. Smith (1978), Anatomy of a Los Angeles smog episode: Pollutant transport in the daytime sea breeze regime, *Atmos. Environ.*, **12**, 893–907, doi:10.1016/0004-6981(78)90028-8.
- Bonan, G. B. (1996), A land surface model (LSM version 1.0) for ecological, hydrological, and atmospheric studies: Technical description and user's guide, 150 pp., Natl. Cent. for Atmos. Res., Boulder, Colo.
- Bonan, G. B., F. S. Chapin III, and S. L. Thompson (1995), Boreal forest and tundra ecosystems as components of the climate system, *Clim. Change*, **29**, 145–168, doi:10.1007/BF01094014.
- Bonan, G. B., K. J. Davis, D. Baldocchi, D. Fitzgerald, and H. Neumann (1997), Comparison of the NCAR LSM I land surface model with BOR-EAS aspen and jack pine tower fluxes, *J. Geophys. Res.*, **102**, 29,065–29,076, doi:10.1029/96JD03095.
- Carreras-Sospedra, M., D. Dabdub, M. Rodriguez, and J. Brouwer (2006), Air quality modeling in the south coast air basin of California: What do the numbers really mean?, *J. Air Waste Manage. Assoc.*, **56**, 1184–1195.
- Conil, S., and A. Hall (2006), Local regimes of atmospheric variability: A case study of southern California, *J. Clim.*, **19**, 4308–4325, doi:10.1175/JCLI3837.1.
- Cooley, H. S., W. J. Riley, M. S. Torn, and Y. He (2005), Impact of agricultural practice on regional climate in a coupled land surface mesoscale model, *J. Geophys. Res.*, **110**, D03113, doi:10.1029/2004JD005160.
- Croes, B. E., and E. M. Fujita (2003), Overview of the 1997 Southern California Ozone Study (SCOS97-NARSTO), *Atmos. Environ.*, **37**, S3–S26, doi:10.1016/S1352-2310(03)00379-0.
- Davison, A. W., and J. D. Barnes (1998), Effects of ozone on wild plants, *New Phytol.*, **139**, 135–151, doi:10.1046/j.1469-8137.1998.00177.x.
- Denning, A. S., G. J. Collatz, C. G. Zhang, D. A. Randall, J. A. Berry, P. J. Sellers, G. D. Colello, and D. A. Dazlich (1996), Simulations of terrestrial carbon metabolism and atmospheric CO<sub>2</sub> in a general circulation model. 1. Surface carbon fluxes, *Tellus, Ser. B*, **48**, 521–542, doi:10.1034/j.1600-0889.1996.t01-2-00009.x.
- Dickinson, R. E., A. Henderson-Sellers, P. J. Kennedy, and M. F. Wilson (1986), Biosphere/atmosphere transfer scheme (BATS) for the NCAR community climate model, *NCAR Tech. Note TN275*, Natl. Cent. for Atmos. Res., Boulder, Colo.
- Dillon, M. B., M. S. Lamanna, G. W. Schade, A. H. Goldstein, and R. C. Cohen (2002), Chemical evolution of the Sacramento urban plume: Transport and oxidation, *J. Geophys. Res.*, **107**(D5), 4045, doi:10.1029/2001JD000969.
- Edinger, J. G. (1973), Vertical distribution of photochemical smog in Los Angeles basin, *Environ. Sci. Technol.*, **7**, 247–252, doi:10.1021/es60075a004.



- EIA (2003), State energy data report, Energy Inf. Admin., U. S. Dep. of Energy, Washington, D. C.
- Fan, S. M., M. Gloor, J. Mahlman, S. Pacala, J. Sarmiento, T. Takahashi, and P. Tans (1998), A large terrestrial carbon sink in North America implied by Atmospheric and oceanic carbon dioxide models, *Science*, **282**, 456–458, doi:10.1126/science.282.5388.442.
- Fenn, M., and A. Bytnerowicz (1997), Summer throughfall and winter deposition in the San Bernardino Mountains in southern California, *Atmos. Environ.*, **31**, 673–683, doi:10.1016/S1352-2310(96)00238-5.
- Fenn, M. E., M. A. Poth, and D. W. Johnson (1996), Evidence for nitrogen saturation in the San Bernardino Mountains in southern California, *For. Ecol. Manage.*, **82**, 211–230, doi:10.1016/0378-1127(95)03668-7.
- Fenn, M., M. Poth, S. Schilling, and D. Grainger (2000), Throughfall and fog deposition of nitrogen and sulfur at an N-limited and N-saturated site in the San Bernardino Mountains, southern California, *Can. J. For. Res.*, **30**, 1476–1488, doi:10.1139/cjfr-30-9-1476.
- Flanner, M. G., C. S. Zender, J. T. Randerson, and P. J. Rasch (2007), Present day climate forcing and response from black carbon in snow, *J. Geophys. Res.*, **112**, D11202, doi:10.1029/2006JD008003.
- Franco, G. (2002), Inventory of California greenhouse gas emissions and sinks: 1990–1999, Calif. Energy Comm., Sacramento, Calif.
- Gerbig, C., J. C. Lin, S. C. Wofsy, B. C. Daube, A. E. Andrews, B. B. Stephens, P. S. Bakwin, and C. A. Grainger (2003), Toward constraining regional-scale fluxes of CO<sub>2</sub> with atmospheric observations over a continent: 1. Observed spatial variability from airborne platforms, *J. Geophys. Res.*, **108**(D24), 4756, doi:10.1029/2002JD003018.
- Grell, G., J. Dudhia, and D. Stauffer (1995), A description of the fifth-generation Penn State/NCAR mesoscale model (MM5), Natl. Cent. for Atmos. Res., Boulder, Colo.
- Grulke, N., and L. Baldum (1999), Deciduous conifers: High N deposition and O<sub>3</sub> exposure effects on growth and biomass allocation in ponderosa pine, *Water Air Soil Pollut.*, **116**, 235–248, doi:10.1023/A:1005227520012.
- Grulke, N., C. Andersen, M. Fenn, and P. Miller (1998), Ozone exposure and nitrogen deposition lowers root biomass of ponderosa pine in the San Bernardino Mountains, California, *Environ. Pollut.*, **103**, 63–73, doi:10.1016/S0269-7491(98)00130-4.
- Grulke, N., C. Andersen, and W. Hogsett (2001), Seasonal changes in above- and belowground carbohydrate concentrations of ponderosa pine along a pollution gradient, *Tree Physiol.*, **21**, 173–181.
- Gurney, K. R., et al. (2002), Towards robust regional estimates of CO<sub>2</sub> sources and sinks using atmospheric transport models, *Nature*, **415**, 626–630, doi:10.1038/415626a.
- Hong, S. Y., and H. L. Pan (1996), Nonlocal boundary layer vertical diffusion in a Medium-Range Forecast Model, *Mon. Weather Rev.*, **124**, 2322–2339, doi:10.1175/1520-0493(1996)124<2322:NBLVDI>2.0.CO;2.
- Hsueh, D. Y., N. Y. Krakauer, J. T. Randerson, X. M. Xu, S. E. Trumbore, and J. R. Southon (2007), Regional patterns of radiocarbon and fossil fuel-derived CO<sub>2</sub> in surface air across North America, *Geophys. Res. Lett.*, **34**, L02816, doi:10.1029/2006GL027032.
- Kalnay, E., et al. (1996), The NCEP/NCAR 40-Year Reanalysis Project, *Bull. Am. Meteorol. Soc.*, **77**, 437–471, doi:10.1175/1520-0477(1996)077<0437:TNYRP>2.0.CO;2.
- Kistler, R., et al. (2001), The NCEP-NCAR 50-year reanalysis: Monthly means CD-ROM and documentation, *Bull. Am. Meteorol. Soc.*, **82**, 247–267, doi:10.1175/1520-0477(2001)082<0247:TNNYRM>2.3.CO;2.
- Lee, E., D. Tingey, W. Hogsett, and J. Laurence (2003), History of tropospheric ozone for the San Bernardino Mountains of southern California, 1963–1999, *Atmos. Environ.*, **37**, 2705–2717, doi:10.1016/S1352-2310(03)00203-6.
- Levin, I., and V. Heshaimer (2000), Radiocarbon - A unique tracer of global carbon cycle dynamics, *Radiocarbon*, **42**, 69–80.
- Levin, I., and B. Kromer (2004), The tropospheric (CO<sub>2</sub>)-C-14 level in mid-latitudes of the Northern Hemisphere (1959–2003), *Radiocarbon*, **46**, 1261–1272.
- Levin, I., R. Graul, and N. B. A. Trivett (1995), Long-term observations of atmospheric CO<sub>2</sub> and carbon isotopes at continental sites in Germany, *Tellus, Ser. B*, **47**, 23–34, doi:10.1034/j.1600-0889.47.issue1.4.x.
- Levin, I., B. Kromer, M. Schmidt, and H. Sartorius (2003), A novel approach for independent budgeting of fossil fuel CO<sub>2</sub> over Europe by (CO<sub>2</sub>)-C-14 observations, *Geophys. Res. Lett.*, **30**(23), 2194, doi:10.1029/2003GL018477.
- Lintner, B. R., W. Buermann, C. D. Koven, and I. Y. Fung (2006), Seasonal circulation and Mauna Loa CO<sub>2</sub> variability, *J. Geophys. Res.*, **111**, D13104, doi:10.1029/2005JD006535.
- Litton, C. M., J. W. Raich, and M. G. Ryan (2007), Carbon allocation in forest ecosystems, *Global Change Biol.*, **13**, 2089–2109, doi:10.1111/j.1365-2486.2007.01420.x.
- Lu, R., and R. P. Turco (1995), Air pollutant transport in a coastal environment. 2. Three-dimensional simulations over Los Angeles basin, *Atmos. Environ.*, **29**, 1499–1518, doi:10.1016/1352-2310(95)00015-Q.
- Marland, G., T. A. Boden, and R. J. Andres (2006), Global, regional, and national CO<sub>2</sub> emissions, in *Trends: A Compendium of Data on Global Change*, Carbon Dioxide Inf. Anal. Cent., Oak Ridge Natl. Lab., U. S. Dep. of Energy, Oak Ridge, Tenn.
- Marr, L. C., D. R. Black, and R. A. Harley (2002), Formation of photochemical air pollution in central California: 1. Development of a revised motor vehicle emission inventory, *J. Geophys. Res.*, **107**(D6), 4047, doi:10.1029/2001JD000689.
- McElroy, J. L., and T. B. Smith (1986), Vertical pollutant distributions and boundary layer structure observed by airborne lidar near the complex southern California coastline, *Atmos. Environ.*, **20**, 1555–1566, doi:10.1016/0004-6981(86)90244-1.
- Miller, P., O. Taylor, and M. Poe (1986), Spatial variation of summer ozone concentrations in the San Bernardino Mountains, paper presented at 79th Annual Meeting of the Air Pollut. Control Assoc., Minneapolis, Minn., 22–27 June.
- Miller, P., A. Bytnerowicz, M. Fenn, M. Poth, P. Temple, S. Schilling, D. Jones, D. Johnson, J. Chow, and J. Watson (1998), Multidisciplinary study of ozone, acidic deposition and climate effects on a mixed conifer forest in California, USA, *Chemosphere*, **36**, 1001–1006, doi:10.1016/S0045-6535(97)10162-X.
- Olivier, J. G. J., J. P. J. Bloos, J. J. M. Berdowski, A. J. H. Visschedijk, and A. F. Bouwman (1999), A 1990 global emission inventory of anthropogenic sources of carbon monoxide on 1 × 1 degree developed in the framework of EDGAR/GEIA, *Chemosphere Global Change Sci.*, **1**, 1–17, doi:10.1016/S1465-9972(99)00019-7.
- Parry, M. L., O. F. Canziani, J. P. Palutikof, V. D. Linden, and C. E. Hansen (Eds.) (2007), *Summary for Policymakers*, Cambridge Univ. Press, Cambridge, UK.
- Peel, J. L., P. E. Tolbert, M. Klein, K. B. Metzger, W. D. Flanders, K. Todd, J. A. Mulholland, P. B. Ryan, and H. Frumkin (2005), Ambient air pollution and respiratory emergency department visits, *Epidemiology*, **16**, 164–174, doi:10.1097/01.ede.0000152905.42113.db.
- Ramanathan, V., P. J. Crutzen, J. T. Kiehl, and D. Rosenfeld (2001), Atmosphere - Aerosols, climate, and the hydrological cycle, *Science*, **294**, 2119–2124, doi:10.1126/science.1064034.
- Randerson, J. T., I. G. Enting, E. A. G. Schuur, K. Caldeira, and I. Y. Fung (2002), Seasonal and latitudinal variability of troposphere Delta (CO<sub>2</sub>)-C-14: Post bomb contributions from fossil fuels, oceans, the stratosphere, and the terrestrial biosphere, *Global Biogeochem. Cycles*, **16**(4), 1112, doi:10.1029/2002GB001876.
- Raphael, M. N. (2003), The Santa Ana winds of California, *Earth Interact.*, **7**, (Available at <http://EarthInteractions.org>)
- Raupach, M., G. Marland, P. Ciais, C. LeQuere, J. Canadell, G. Klepper, and C. Field (2007), Global and regional drivers of accelerating CO<sub>2</sub> emissions, *Proc. Natl. Acad. Sci. U. S. A.*, **104**, 10,288–10,293, doi:10.1073/pnas.0700609104.
- Riley, W. J., C. J. Still, B. R. Helliker, M. Ribas-Carbo, and J. A. Berry (2003), <sup>18</sup>O composition of CO<sub>2</sub> and H<sub>2</sub>O ecosystem pools and fluxes in a tallgrass prairie: Simulations and comparisons to measurements, *Global Change Biol.*, **9**, 1567–1581, doi:10.1046/j.1365-2486.2003.00680.x.
- Riley, W. J., J. T. Randerson, P. N. Foster, and T. J. Lueker (2005), The influence of terrestrial ecosystems and topography on coastal CO<sub>2</sub> measurements: A case study at Trinidad Head, California, *J. Geophys. Res.*, **110**, G01005, doi:10.1029/2004JG000007.
- Rinehart, L. R., E. M. Fujita, J. C. Chow, K. Magliano, and B. Zielinska (2006), Spatial distribution of PM<sub>2.5</sub> associated organic compounds in central California, *Atmos. Environ.*, **40**, 290–303, doi:10.1016/j.atmosenv.2005.09.035.
- Rosenfeld, D., and A. Givati (2006), Evidence of orographic precipitation suppression by air pollution-induced aerosols in the western United States, *J. Appl. Meteorol. Climatol.*, **45**, 893–911, doi:10.1175/JAM2380.1.
- Santos, G. M., J. R. Southon, K. C. Druffel-Rodriguez, S. Griffin, and M. Mazon (2004), Magnesium perchlorate as an alternative water trap in AMS graphite sample preparation: A report on sample preparation at KCCAMS at the Univ. of California, Irvine, *Radiocarbon*, **46**, 165–173.
- Schwartz, J., D. W. Dockery, and L. M. Neas (1996), Is daily mortality associated specifically with fine particles?, *J. Air Waste Manage. Assoc.*, **46**, 927–939.
- Schwarzenegger, A. (2005), Governor of the State of California Executive Order, S-3-05, Executive Dep. of Calif., Sacramento, 1 June.
- Sellers, P. J., D. A. Randall, C. J. Collatz, J. A. Berry, C. B. Field, D. A. Dazlich, C. Zhang, and G. D. Colello (1996), A revised land surface parameterization (SiB2) for atmospheric GCMs. Part 1: Model formulation, *J. Clim.*, **9**, 676–705, doi:10.1175/1520-0442(1996)009<0676:ARLSPF>2.0.CO;2.



- Stephens, B., et al. (2007), Weak northern and strong tropical land carbon uptake from vertical profiles of atmospheric CO<sub>2</sub>, *Science*, 316, 1732–1735, doi:10.1126/science.1137004.
- Stern, N. (2006), *Stern Review on the Economics of Climate Change*, Cambridge Univ. Press, Cambridge, UK.
- Stuiver, M., and H. A. Polach (1977), Reporting of C-14 data - Discussion, *Radiocarbon*, 19, 355–363.
- Thompson, M. V., and J. T. Randerson (1999), Impulse response functions of terrestrial carbon cycle models: Method and application, *Global Change Biol.*, 5, 371–394, doi:10.1046/j.1365-2486.1999.00235.x.
- Turnbull, J. C., J. B. Miller, S. J. Lehman, P. P. Tans, R. J. Sparks, and J. Southon (2006), Comparison of <sup>14</sup>CO<sub>2</sub>, CO, and SF<sub>6</sub> as tracers for recently added fossil fuel CO<sub>2</sub> in the atmosphere and implications for biological CO<sub>2</sub> exchange, *Geophys. Res. Lett.*, 33, L01817, doi:10.1029/2005GL024213.
- Waring, R. H., J. J. Landsberg, and M. Williams (1998), Net primary production of forests: A constant fraction of gross primary production?, *Tree Physiol.*, 18, 129–134.
- Westerling, A. L., D. R. Cayan, T. J. Brown, B. L. Hall, and L. G. Riddle (2004), Climate, Santa Ana winds, and autumn wildfires in southern California, *Eos Trans. AGU*, 85, 289–300, doi:10.1029/2004EO310001.
- Wofsy, S. C., and R. C. Harris (2002), The North American Carbon Program (NACP), 56 pp., U.S. Global Change Res. Program, Washington, D. C.
- 
- M. L. Fischer, Energy and Environment Division, E. O. Lawrence Berkeley National Laboratory, Berkeley, CA 94720, USA.
- M. L. Goulden, D. E. Pataki, and J. T. Randerson, Earth System Science Department, University of California, Croul Hall, Irvine, CA 92697, USA.
- J. G. Hatch, Brightworks LLC, 123 NW 12th Avenue, Suite 239, Portland, OR 97209, USA.
- D. Y. Hsueh, Department of Ecology, Evolution, and Environmental Biology, Columbia University, New York, NY 10027, USA.
- W. J. Riley, Earth Sciences Division, E. O. Lawrence Berkeley National Laboratory, 90-1106, 1 Cyclotron Road, Berkeley, CA 94720, USA. (wjrliley@lbl.gov)
- W. Wang, Department of Ecology and Evolutionary Biology, University of California, Irvine, CA 92697, USA.